



Gallagher-Moszkowski splitting in deformed odd-odd nuclei within a microscopic approach

L. Bonneau,^{1,*} N. Kontowicz,¹ J. Bartel,² H. Moliqeu,² Meng-Hock Koh (辜明福) ,^{3,4} and N. Minkov ⁵

¹*LP2i Bordeaux, UMR 5797, Université de Bordeaux, CNRS, F-33170 Gradignan, France*

²*IPHC, UMR 7178, Université de Strasbourg, CNRS, F-67000 Strasbourg, France*

³*Department of Physics, Faculty of Science, Universiti Teknologi Malaysia, 81310 Johor Bahru, Johor, Malaysia*

⁴*UTM Centre for Industrial and Applied Mathematics, 81310 Johor Bahru, Johor, Malaysia*

⁵*Institute of Nuclear Research and Nuclear Energy, Bulgarian Academy of Sciences, Tzarigrad Road 72, BG-1784, Sofia, Bulgaria*



(Received 26 February 2024; accepted 10 April 2024; published 3 May 2024)

Background: Low-lying bandhead states in axially prolate deformed odd-odd nuclei have long been described essentially within the rotor+two-quasiparticle picture. This approach allows one to explain the appearance of so-called Gallagher-Moszkowski doublets of bandheads with $K = \Omega_n \pm \Omega_p$, sum and difference of neutron and proton angular momentum projections on the symmetry axis. According to an empirical rule stated by Gallagher and Moszkowski the spin-aligned configuration lies lower in energy than the spin-antialigned configuration. A recent study by Robledo, Bernard, and Bertsch [*Phys. Rev. C* **89**, 021303(R) (2014)] within the Gogny energy-density functional with self-consistent blocking of the unpaired nucleons showed that calculations fail to reproduce this rule in about half of the cases, and points to the density-dependent term of the functional as responsible of this failure.

Purpose: In this paper we aim at pushing further this analysis to exhibit the mechanism underlying the energy splitting in a Gallagher-Moszkowski doublet.

Method: We work in the framework of the Skyrme energy-density functional approach, including BCS pairing correlations with self-consistent blocking. We use the SIII parametrization with time-odd terms and seniority pairing matrix elements extending a previous study of K -isomeric states in even-even nuclei [*Phys. Rev. C* **105**, 044329 (2022)].

Results: We find that the energy splitting results from a competition between the spin-spin, density-dependent, and current-current terms of the Skyrme energy-density functional.

Conclusions: In doublets where the larger K value is lower in energy the Gallagher-Moszkowski rule is always satisfied by the SIII Skyrme energy-density functional. In doublets, in contrast, where the smaller K value lies lower, the energy splittings are calculated to be rather small, and often a disagreement with the Gallagher-Moszkowski rule occurs.

DOI: [10.1103/PhysRevC.109.054303](https://doi.org/10.1103/PhysRevC.109.054303)

I. INTRODUCTION

Deformed doubly-odd nuclei have long been described within the rotor+two-quasiparticle picture as a rotating core coupled through the so-called Coriolis term to one neutron and one proton moving in a spheroidal mean field [1]. Axial deformation in such nuclei provides K , the projection on the symmetry axis of the intrinsic angular momentum, as a good quantum number. In the deformation-alignment scheme, the core rotates around an axis orthogonal to the symmetry axis of the nucleus and the projection on the symmetry axis of the total angular momentum of the nucleus is thus equal to K . Moreover K is the sum of the neutron Ω_n and the proton Ω_p angular momentum projections on the symmetry axis (see Fig. 1). Bohr and Mottelson [1] and Peker [2] showed that the ground-state angular momentum of many deformed odd-odd nuclei can be accounted for by the coupling of the unpaired proton and neutron angular momenta. Gallagher and Moszkowski

then proposed in Ref. [3] a spin-spin coupling rule to determine whether the lower lying configuration corresponds to $\Omega_n + \Omega_p$ or $|\Omega_n - \Omega_p|$. According to this rule, the lower-lying configuration is the one in which spins of the neutron and the proton are parallel. This rule is remarkably successful as, even to date, it suffers from only one exception, in the ^{166}Ho nucleus. As reviewed by Boisson *et al.* [4], this success was accompanied by several early theoretical investigations [5–7] to understand its origin in terms of the residual interaction between the unpaired neutron and proton in the framework of the two-quasiparticle+rotor model. About two decades later, Jain and collaborators provided in Ref. [8] a comprehensive review of the structure of deformed odd-odd rare-earth nuclei, including a systematic analysis of the neutron-proton residual interaction in the two-quasiparticle+rotor model. Note however, that the work published shortly before Ref. [8] by Covello and collaborators on the tensor contribution to the neutron-proton residual interaction, in the same two-quasiparticle + rotor model [9], was not mentioned in Ref. [8]. More recently two systematic studies of odd-odd nuclei were performed. On the one hand Robledo, Bernard, and Bertsch [10] investigated

*Corresponding author: bonneau@lp2ib.in2p3.fr

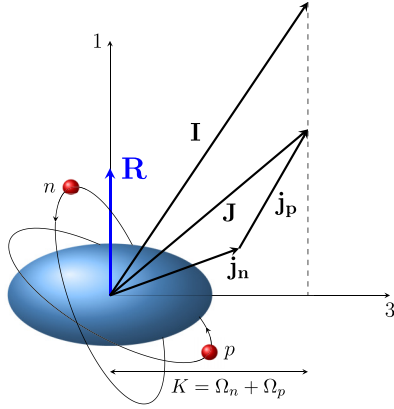


FIG. 1. Schematic representation of collective \mathbf{R} , intrinsic $\mathbf{J} = \mathbf{j}_n + \mathbf{j}_p$, and total $\mathbf{I} = \mathbf{R} + \mathbf{J}$ angular momenta in an axially deformed odd-odd nucleus within the deformation-alignment scheme.

the Gallagher-Moszkowski splitting with the Gogny energy-density functional (EDF) with self-consistent blocking. They identified the density-dependent term of the functional as being responsible for the disagreement with the Gallagher-Moszkowski rule where it occurred. On the other hand Ward and collaborators [11] performed systematic calculations of ground-state spins and parities of odd-odd nuclei across the nuclear chart within the macroscopic-microscopic finite-range droplet model combined with a two-quasiparticle+rotor model with various residual interactions.

Overall very few EDF based calculations in deformed odd-odd nuclei have been performed so far. In Ref. [12] Bennour and collaborators studied the spectroscopic properties of axially deformed doubly-odd nuclei in the rare-earth and actinide regions in the two-quasiparticle+rotor picture with Skyrme-EDF intrinsic solutions. The SIII parametrization of the effective Skyrme interaction was used to generate the neutron and proton quasiparticle energies and their interaction matrix elements (playing the role of the neutron-proton residual interaction). More precisely they described the band-head states of the considered odd-odd nuclei by the creation of two quasiparticles on the (fully paired) Hartree-Fock-BCS ground state of a neighboring even-even nucleus. In contrast Robledo and collaborators [10] later used the Gogny EDF with self-consistent blocking (SCB), hence breaking the time-reversal symmetry at the one-body level. In the present paper we extend the recent study of two-quasiparticle states in even-even nuclei [13] within the Skyrme-EDF framework with BCS pairing and self-consistent blocking to deformed odd-odd nuclei. Even though several codes based on Skyrme EDF with superior capabilities already exist [14–16], we are not aware of any published applications to deformed doubly-odd nuclei dedicated to the Gallagher-Moszkowski splitting, neither within the Skyrme nor within the Gogny EDF, after those of Ref. [10].

In the present work we focus on Gallagher-Moszkowski doublets and aim at understanding the mechanism of their energy splitting within the Skyrme-EDF framework with BCS pairing and self-consistent blocking, pushing further the analysis performed by Robledo and collaborators [10]. Because

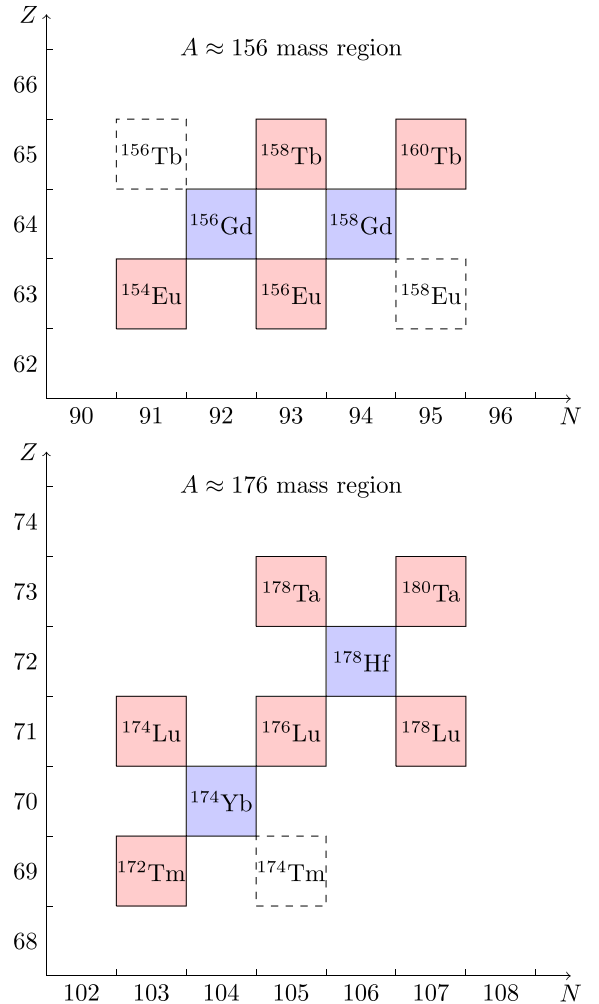


FIG. 2. Portions of the nuclide chart in the vicinity of studied rare-earth nuclei. Dashed boxes represent odd-odd nuclei for which too few data are available and are thus not studied here.

we focus on deciphering the microscopic mechanism at work behind the Gallagher-Moszkowski empirical rule, we do not perform our study on a systematic basis, but in selected strongly deformed nuclei in two mass regions and for which sufficient data on Gallagher-Moszkowski doublets are experimentally known:

- (i) rare-earth mass region and beyond: odd-odd nuclei surrounding the even-even $^{156,158}\text{Gd}$, ^{174}Yb , and ^{178}Hf nuclei (see Fig. 2);
- (ii) actinide mass region between $A \approx 230$ and $A \approx 250$: odd-odd nuclei surrounding the even-even nuclei $^{230,232}\text{Th}$, $^{240,242}\text{Pu}$, and $^{250,252}\text{Cf}$ (see Fig. 3).

After a brief presentation of the theoretical framework and calculational details in the next section, we present in Sec. III the resulting bandhead spectra obtained within self-consistent blocking for the Gallagher-Moszkowski doublets known experimentally. Then we show the relevance of perturbative blocking for the investigation of the splitting mechanism in Sec. IV. Finally we draw conclusions and give perspectives in Sec. V.

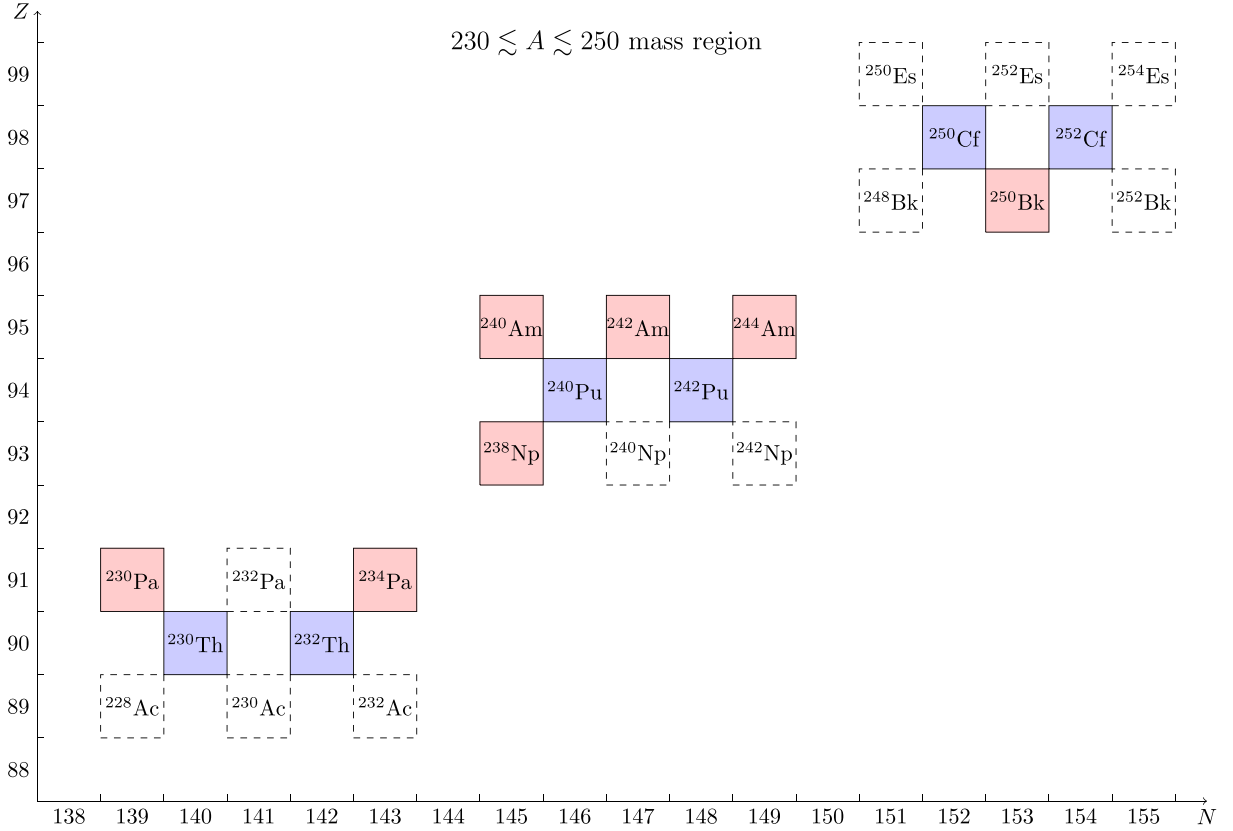


FIG. 3. Same as Fig. 2 for the actinide nuclei of interest.

II. THEORETICAL FRAMEWORK AND CALCULATIONAL DETAILS

All two-quasiparticle states of the considered nuclei are assumed to have axially symmetric and left-right symmetric shapes in the intrinsic (body-fixed) frame. They are described within the Skyrme+BCS energy-density functional with self-consistent blocking (of one neutron and one proton single-particle states) as explained in Ref. [17]. As in a previous study of K -isomeric two-quasiparticle states [13] we use the SIII parametrization [18] of the Skyrme energy-density functional and constant pairing matrix elements (often called “seniority” or BCS pairing interaction).

Because of the self-consistent blocking, time-reversal symmetry is broken at the one-body level and the Kramers degeneracy is removed in the single-particle energy spectrum. Moreover, as explained in Refs. [17,19], we work in the “minimal” scheme of the SIII Skyrme parametrization, in which the only time-odd fields retained in the Hartree-Fock Hamiltonian are the spin and current vector fields. Including the other terms would introduce a bias as they are accompanied by terms involving time-even densities that were not taken into account in the SIII fitting protocol [18]. In the notation of the Appendix of Ref. [19] this corresponds to keeping the B_3 (current-current) term, B_9 (spin-orbit) term, $B_{10,11}$ (spin-spin) terms, and $B_{12,13}$ (density-dependent spin-spin) terms.

The pairing contribution to the energy-density functional is calculated from the expectation value of the pairing interaction in a BCS state including blocking. The parametrization

of the nucleon-number dependence of the pairing matrix elements is the same as in Ref. [17] and the fitting protocol of their strength is presented in Refs. [13,20]. In this work we use the same values as in Ref. [20] for the nuclei around $A = 178$ ($^{174,176,178}\text{Lu}$, $^{178,180}\text{Ta}$) and the same values as in Ref. [13] for the actinide nuclei ($^{230,234}\text{Pa}$, ^{238}Np , ^{242}Am and ^{250}Bk). In the medium-heavy rare-earth nuclei around $A = 156$, we adjust the neutron pairing strength parameter G_n to the first 2^+ excitation energy in ^{156}Gd , keeping that of protons G_p equal to $0.9 \times G_n$ as done in the other mass regions (see Ref. [20] for a precise definition of G_n and G_p). This observable is shown in Ref. [20] to be a relevant measure of pairing correlations equivalent to the odd-even binding-energy differences. We find $G_n = 17.1$ MeV. The BCS equations are then solved for all single-particle states with a smearing factor $f(e_i) = \{1 + \exp[(e_i - X - \lambda_q)/\mu]\}^{-1}$ where e_i is the energy of the single-particle state $|i\rangle$, X plays the role of a cutoff factor with $X = 6$ MeV, λ_q is the chemical potential for the charge state $q = n, p$, and $\mu = 0.2$ MeV is a diffuseness parameter.

Finally the single-particle states are expanded in a truncated cylindrical harmonic-oscillator basis with parity symmetry. In nuclei around $A = 178$, we use the same basis parameters as in Ref. [20] and in actinides we take the parameters of Ref. [13]. Around $A = 156$, the optimal basis parameters are found to be $b = 0.495$ and $q = 1.18$ in the notation of Ref. [21], with $N_0 + 1 = 15$ spherical oscillator major shells. As in Ref. [13] all integrations are performed by Gauss-Hermite quadratures with 30 mesh points in the z

direction of the symmetry axis and Gauss-Laguerre quadratures with 15 mesh points in a direction orthogonal to the symmetry axis.

III. RESULTS FOR BANDHEAD SPECTRA

In this section we report on the bandhead spectra calculated within the SIII Skyrme energy-density functional with self-consistent blocking as explained above, and we present the results by mass region. We report only on experimentally observed Gallagher-Moszkowski doublets, and for each studied odd-odd nucleus we take the two-quasiparticle K^π configuration of the experimental ground state as a reference state to build the energy spectrum of calculated doublets. For completeness we also give the lowest-energy calculated bandhead when it is not among observed Gallagher-Moszkowski doublets.

A. Rare-earth nuclei around $A = 156$

The odd-odd nuclei surrounding the $^{156,158}\text{Gd}$ isotopes are described by two-quasiparticle configurations with respect to the ground state of these even-even nuclei. Sufficient experimental data on Gallagher-Moszkowski doublets are available in $^{154,156}\text{Eu}$ and $^{158,160}\text{Tb}$. It is worth noting that the ^{160}Tb nucleus was studied in Ref. [12], where calculations in the rotor+two-quasiparticle picture with Skyrme-EDF intrinsic solutions were compared with experimental data for several Gallagher-Moszkowski doublets.

First we show in Fig. 4 the neutron and proton single-particle spectra calculated in the ground state of the ^{156}Gd nucleus as an example. In the neutron single-particle spectrum, the second largest cylindrical harmonic-oscillator contribution to the $1/2^+$ state around $e = -9$ MeV has $[400] \uparrow$ Nilsson quantum numbers, in addition to the $[640] \uparrow$ contribution displayed in Fig. 4. From a theoretical point of view we thus expect low-lying bandhead states (up to about 1 MeV excitation energy) in neighboring odd-odd nuclei with configurations involving on the one hand the $11/2^- [505] \uparrow$, $1/2^+ ([640] \uparrow \text{ or } [400] \uparrow)$, $3/2^+ [651] \uparrow$, $3/2^- [521] \uparrow$, $5/2^+ [642] \uparrow$, $5/2^- [523] \downarrow$ neutron single-particle states, and, on the other hand, the $5/2^+ [413] \downarrow$, $5/2^- [532] \uparrow$, $3/2^+ [411] \uparrow$, $7/2^+ [404] \downarrow$ proton single-particle states.

$^{154,156}\text{Eu}$ nuclei ($Z = 63$ and $N = 91, 93$). In panel (a) of Fig. 5 we display the bandhead spectrum of ^{154}Eu restricted to the four Gallagher-Moszkowski doublets experimentally observed. Theoretical excitation energies are all calculated with respect to the $K^\pi = 3^-$ state with the configuration $(11/2^- [505] \uparrow)_n (5/2^+ [413] \downarrow)_p$, which corresponds to the experimental ground state. Overall the energy ordering of calculated doublets follows the expectation from the Koopmans approximation, except for the $(4^+, 1^+)$ doublet built on the $(3/2^+ [651] \uparrow)_n (5/2^+ [413] \downarrow)_p$ configuration, calculated to lie below the $K^\pi = 3^-$ reference state. This suggests that, in the neutron single-particle spectrum, the $11/2^- [505]$ level should be located above the $3/2^+ [651]$ level. While experimental excitation energies are all below 300 keV, the calculated bandhead states of the considered doublets, except

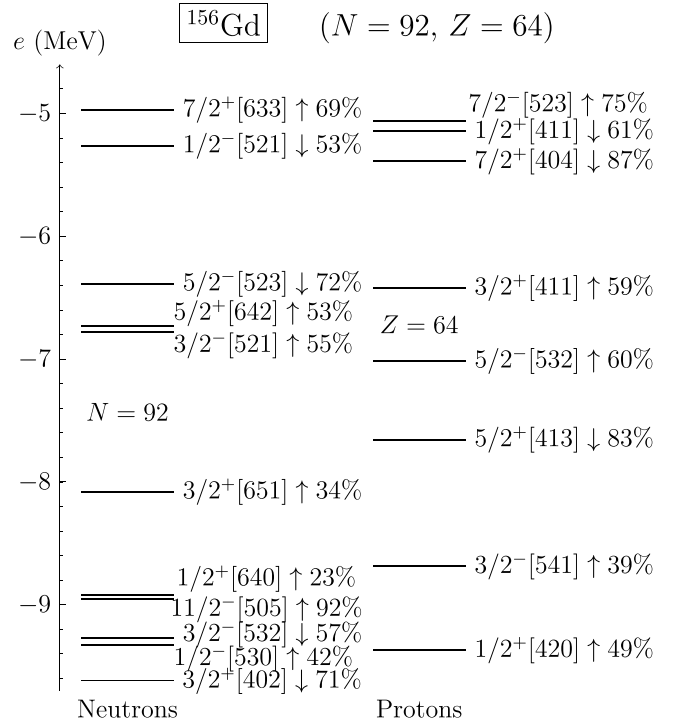


FIG. 4. Neutron and proton single-particle energies e (in MeV) calculated in the ground state of ^{156}Gd , ^{158}Gd . The dominant Nilsson quantum numbers and the weight of the corresponding contribution are indicated. Up and down arrows correspond respectively to spin projections $+1/2$ and $-1/2$ (in \hbar unit) on the symmetry axis.

the discrepant one, agree with experimental data within less than 200 keV, which can be deemed a rather good result.

With the addition of two neutrons to the previous nucleus, the lowest energy configurations of ^{156}Eu are now expected to involve the $3/2^-$ or $5/2^+$ neutron state together with the $5/2^-$ or $5/2^+$ proton state. The resulting four doublets turn out to be precisely the ones experimentally observed. They are displayed in panel (b) of Fig. 5, where the excitation energies are defined with respect to the experimental ground state $K^\pi = 0^+$ with configuration $(5/2^+ [642] \uparrow)_n (5/2^+ [413] \downarrow)_p$. Again the calculated excitation energies agree rather well with the experimental ones, with a discrepancy below 200 keV except for the $K^\pi = 5^-$ state, which is found to be the theoretical ground state almost 300 keV below the $K^\pi = 0^+$ state. This results from the position of the $5/2^-$ level above the $5/2^+$ level in the proton single-particle spectrum consistently with the above discussion for the ^{154}Eu nucleus.

As discussed in Ref. [8], the octupole degree of freedom is expected to play a role in ^{154}Eu , maybe less so in ^{156}Eu . However, according to Afanasjev and Ragnarsson [22], the existence of static octupole deformation in this nucleus (and neighboring nuclei) is not supported by Woods-Saxon calculations of polarization energies of octupole-driving orbitals. Later, systematic axial reflection-asymmetric calculations within the covariant density functional theory [23] showed that even-even neighbors of the odd-odd $^{154,156}\text{Eu}$ isotopes do not have octupole ground-state shape. Finally, a recent global survey of pear-shaped even-even nuclei within

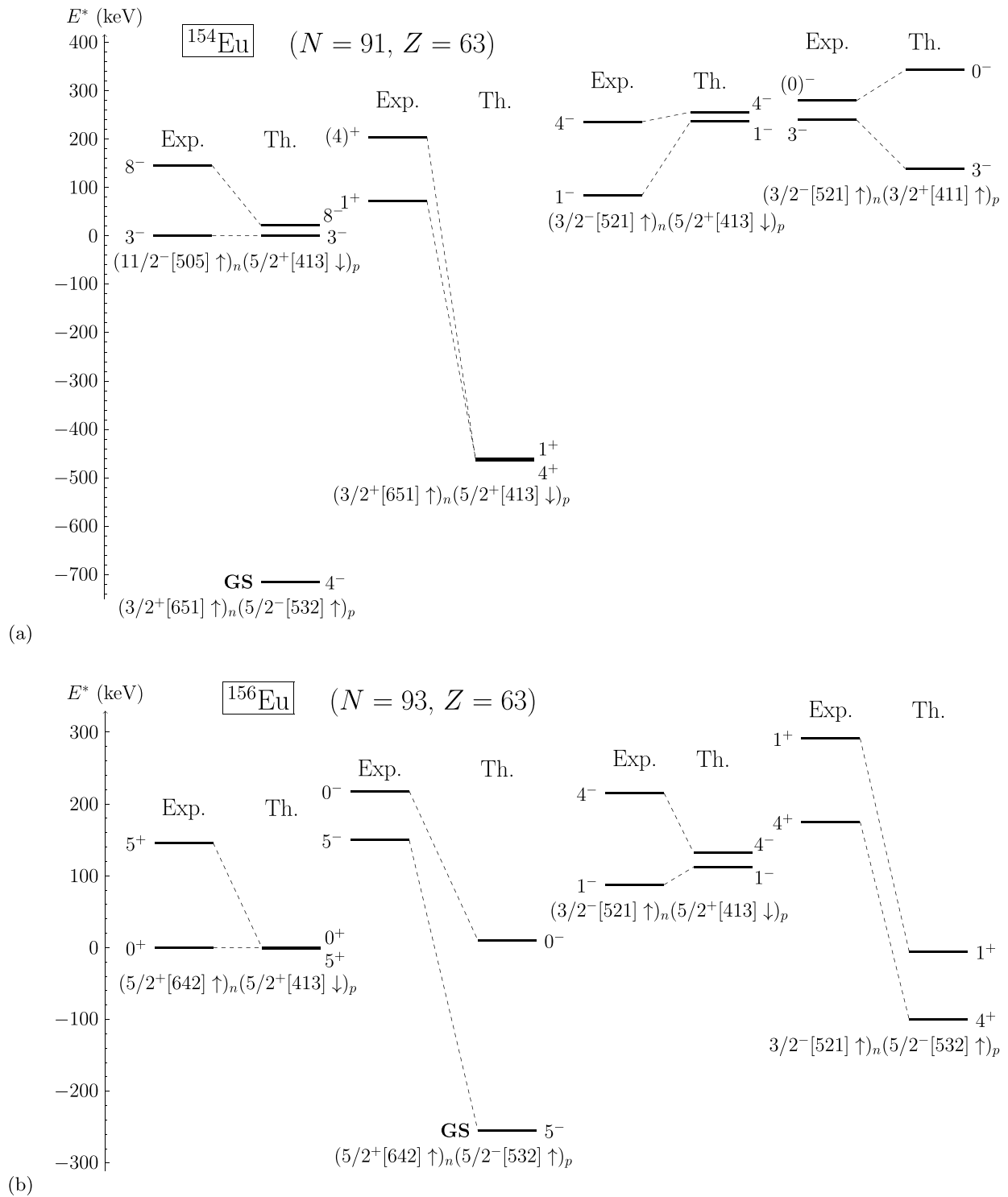


FIG. 5. Bandhead spectra of ^{154}Eu (a) and ^{156}Eu (b) restricted to Gallagher-Moszkowski doublets experimentally observed. For each doublet the left level bars correspond to experiment (labeled “Exp.”), while the right ones correspond to the SCB calculations (labeled “Th. (SCB)”).

nonrelativistic and relativistic EDF approaches [24] lead to the same conclusion. Even if we did not break intrinsic parity to incorporate the octupole degree of freedom in the studied odd-odd nuclei, the basic ingredients for a proper description of bandhead states of two-quasiparticle character are present in our approach, especially the “parity” doublets of single-

neutron and single-proton states with $\Omega_{n,p} = 3/2$ and $\Omega_{n,p} = 5/2$ giving rise to the $(4, 1)^\pm$ doublets in $^{154,156}\text{Eu}$ and $(5, 0)^\pm$ in ^{156}Eu .

$^{158,160}\text{Tb}$ nuclei ($Z = 65$ and $N = 93, 95$). The bandhead spectrum for the six experimentally observed Gallagher-Moszkowski doublets in the ^{158}Tb nucleus is displayed in

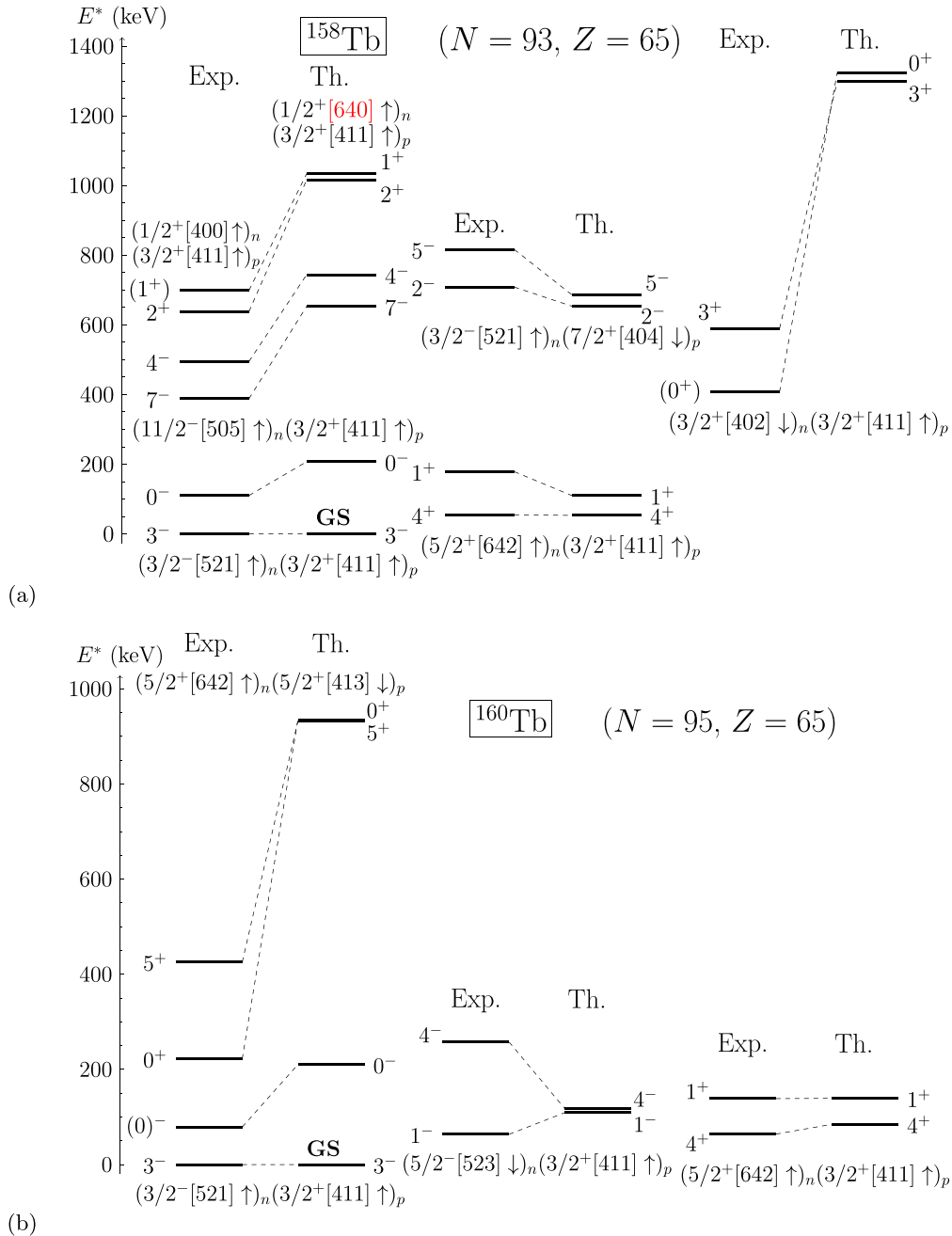


FIG. 6. Same as Fig. 5 for the ^{158}Tb (a) and ^{160}Tb (b) nuclei.

Fig. 6. Note that, in ^{158}Tb , the $1/2^+$ neutron single-particle state involved in the calculated $(2^+, 1^+)$ doublet closest to the experimental one is the $1/2^+[640]$ instead of the $1/2^+[400]$ proposed in Ref. [25].

The theoretical ground state $K^\pi = 3^-$ and first excited bandhead state $K^\pi = 4^+$, both involving the $3/2^+$ proton single-particle level just above the proton Fermi level of ^{156}Gd , agree very well with the experimental ones. The very small excitation energy of the 4^+ state confirms the quasidegeneracy of the $3/2^-$ and $5/2^+$ levels seen in the neutron single-particle spectrum of ^{156}Gd . Moreover the rather good position of the theoretical $(2^-, 5^-)$ doublet seems to indicate

a correct shell gap between the $3/2^+$ and $7/2^+$ levels in the proton single-particle spectrum in ^{156}Gd .

In contrast the doublets involving the $11/2^-$ or $1/2^+$ neutron states are calculated to be too high, which is consistent with too low $11/2^-$ or $1/2^+$ levels around -9 MeV in the neutron single-particle spectrum of ^{156}Gd . Similarly the $(0^+, 3^+)$ doublet calculated with a too large excitation energy suggests that the $3/2^+[402]$ neutron state is too far below the $3/2^-[521]$ state.

The bandhead spectrum for the four experimentally observed Gallagher-Moszkowski doublets in the ^{160}Tb nucleus is displayed in the bottom panel of Fig. 6. Similarly to what

has been obtained in the ^{158}Tb nucleus, the ground state is found to be the 3^- state in agreement with experiment, and the excitation energies of the 4^+ , 1^+ , and 1^- are in excellent agreement with the experimental ones. Apart from the $(5^+, 0^+)$ doublet, for which the discrepancy is of the order of 600 keV, the remaining excitation energies are reproduced within less than the typical 200 keV.

The overall picture emerging from the energy spectra of these odd-odd nuclei around $^{156,158}\text{Gd}$ is that the single-particle states with the quantum numbers relevant for the low-lying two-quasiparticle bandhead states and Gallagher-Moszkowski doublets are present around the neutron and proton Fermi levels in the region $88 \leq N \leq 98$ and $62 \leq Z \leq 68$. However some single-particle hole states appear too high and are expected to generate bandhead states experimentally unobserved in the low-lying spectrum of the considered odd-odd nucleus.

B. Rare-earth nuclei around $A = 176$

The odd-odd nuclei surrounding ^{174}Yb and ^{178}Hf are described by two-quasiparticle configurations with respect to the ground state of these even-even nuclei. A lot of experimental data on Gallagher-Moszkowski doublets are available in ^{172}Tm , $^{174,176,178}\text{Lu}$, and $^{178,180}\text{Ta}$ nuclei.

First we show in Fig. 7 the neutron and proton single-particle spectra calculated in the ground state of the ^{174}Yb and ^{178}Hf nuclei. We expect low-lying bandhead states (up to about 1 MeV excitation energy) in neighboring odd-odd nuclei with configurations involving on the one hand the $7/2^+[633] \uparrow$, $5/2^- [512] \uparrow$, $7/2^- [514] \downarrow$, $9/2^+[624] \uparrow$ neutron single-particle states, and, on the other hand, the $7/2^- [523] \uparrow$, $1/2^+[411] \downarrow$, $7/2^+[404] \downarrow$, $9/2^- [514] \uparrow$, $5/2^+[402] \uparrow$, $1/2^- [541] \downarrow$ proton single-particle states.

^{172}Tm and ^{174}Lu nuclei ($N = 103$ and $Z = 69, 71$). The bandhead spectra for the experimentally observed Gallagher-Moszkowski doublets in the ^{172}Tm and ^{174}Lu nuclei are displayed in Fig. 8. Theoretical excitation energies of ^{172}Tm are all calculated with respect to the $K^\pi = 2^-$ state with the configuration $(5/2^- [512] \uparrow)_n(1/2^+[411] \downarrow)_p$, which corresponds to the experimental ground state, whereas in ^{174}Lu the calculated ground state is the $K^\pi = 1^-$ state in agreement with experiment with the configuration $(5/2^- [512] \uparrow)_n(7/2^+[404] \downarrow)_p$. Overall the calculated excitation energies in these two nuclei agree with experimental data within less than about 200 keV with the notable exception of the $(0^-, 1^-)$ doublet in ^{172}Tm with an overestimation of about 450 keV. The corresponding configuration differs from that of the ground state by the $1/2^- [521]$ neutron state, which suggests that this calculated $1/2^-$ neutron state lies too far below the $5/2^- [512]$ state.

$^{176,178}\text{Lu}$ ($N = 105, 107$ and $Z = 71$) and $^{178,180}\text{Ta}$ nuclei ($N = 105, 107$ and $Z = 73$). The bandhead spectra for the experimentally observed Gallagher-Moszkowski doublets in the $^{176,178}\text{Lu}$ and $^{178,180}\text{Ta}$ nuclei surrounding the even-even ^{178}Hf nucleus are displayed in Figs. 9–11.

The ^{176}Lu nucleus is the experimentally most studied one with 12 observed doublets and with configurations assigned in Refs. [26,27]. Its ground state with $K^\pi = 7^-$ is reproduced by

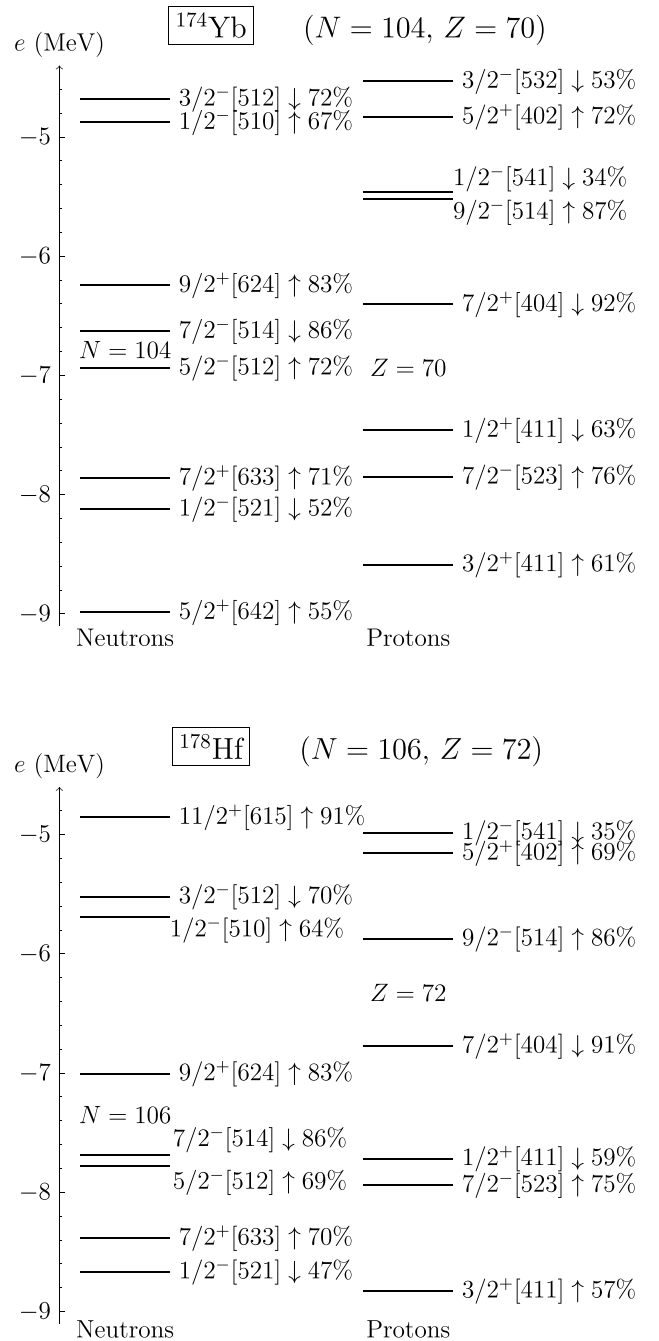


FIG. 7. Same as Fig. 4 for ^{174}Yb and ^{178}Hf .

our calculations. Excellent agreement of calculated excitation energies with experimental data is obtained for the following Gallagher-Moszkowski doublets and configurations:

$$(1^+, 8^+), (9/2^+[624] \uparrow)_n(7/2^+[404] \downarrow)_p;$$

$$(0^+, 7^+), (7/2^- [514] \downarrow)_n(7/2^- [523] \uparrow)_p;$$

$$(4^-, 3^-), (7/2^- [514] \downarrow)_n(1/2^+[411] \downarrow)_p.$$

From the agreements for the last two doublets, we can deduce that $7/2^- [523]$ and $1/2^+[411]$ proton states are correctly

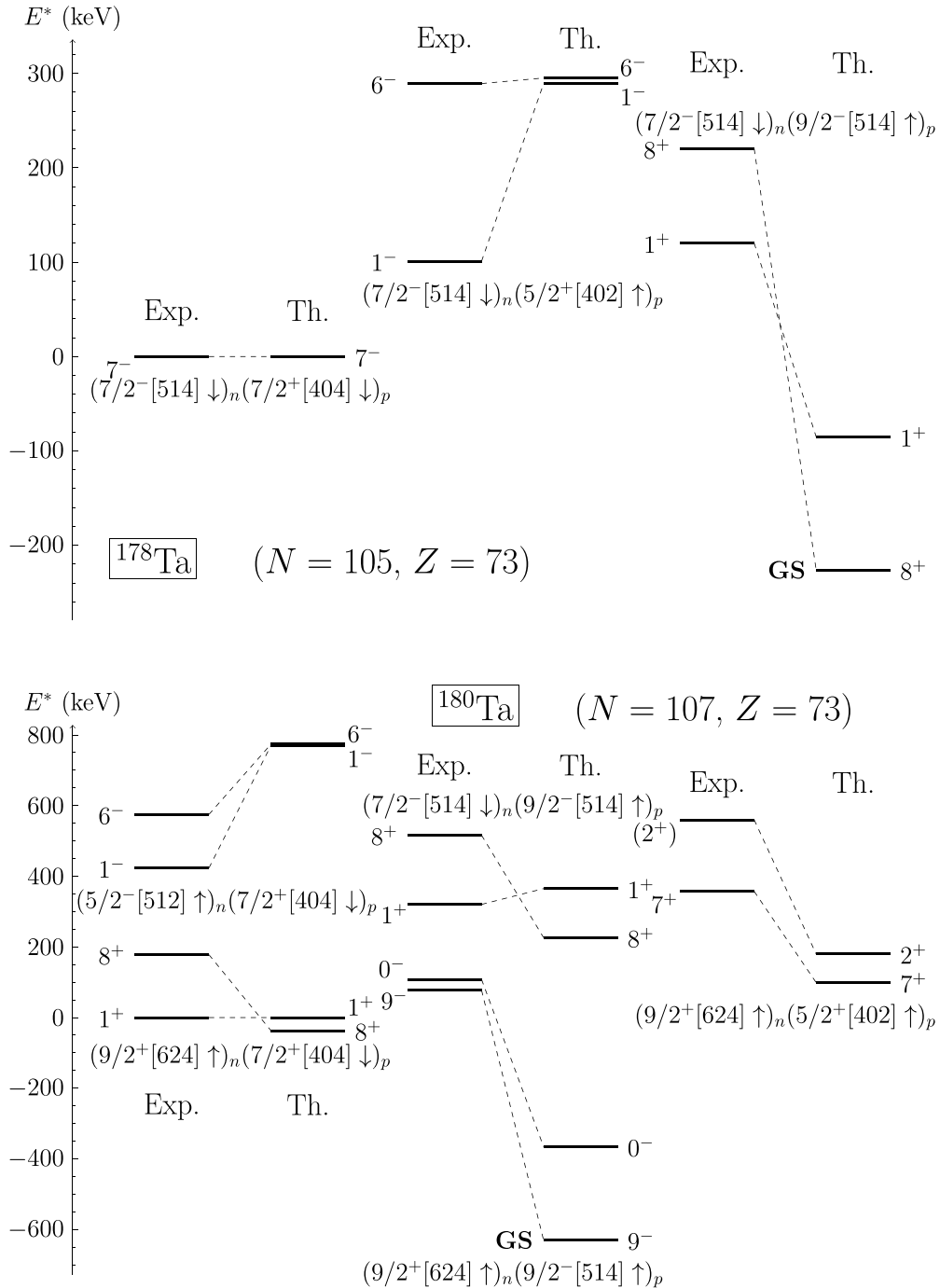


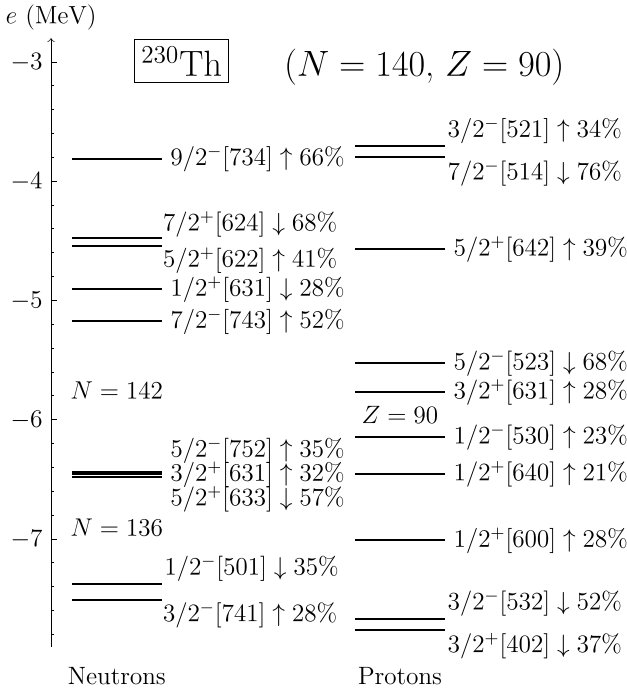
FIG. 11. Same as Fig. 5 for ^{178}Ta and ^{180}Ta nuclei. In ^{178}Ta the ground state is taken to be the 7^- state as in Refs. [28,29] and we use the excitation energy of the 1^+ isomer estimated from systematics 100 keV given by Ref. [29].

octupole degree of freedom is beyond the scope of our calculations.

$^{230,234}\text{Pa}$ nuclei. Figure 14 shows the spectra of these two protactinium isotopes. Note that the calculated doublet (2^+ , 1^+) in ^{230}Pa is built on the $(3/2^- [741] \uparrow)_n (1/2^- [530] \uparrow)_p$ configuration and agrees well with experimental data which had been tentatively interpreted as a $(3/2^- [501] \uparrow)_n (1/2^- [530] \uparrow)_p$ configuration in Ref. [31]. In the neutron single-particle spectrum of ^{230}Th , a $3/2^- [501] \uparrow$ neutron hole state lies about 0.5 MeV below the $3/2^- [741]$ state

and does not appear in Fig. 12. Therefore the configuration $(3/2^- [501] \uparrow)_n (1/2^- [530] \uparrow)_p$ is expected to yield much larger excitation energies for the members of the corresponding (2^+ , 1^+) doublet.

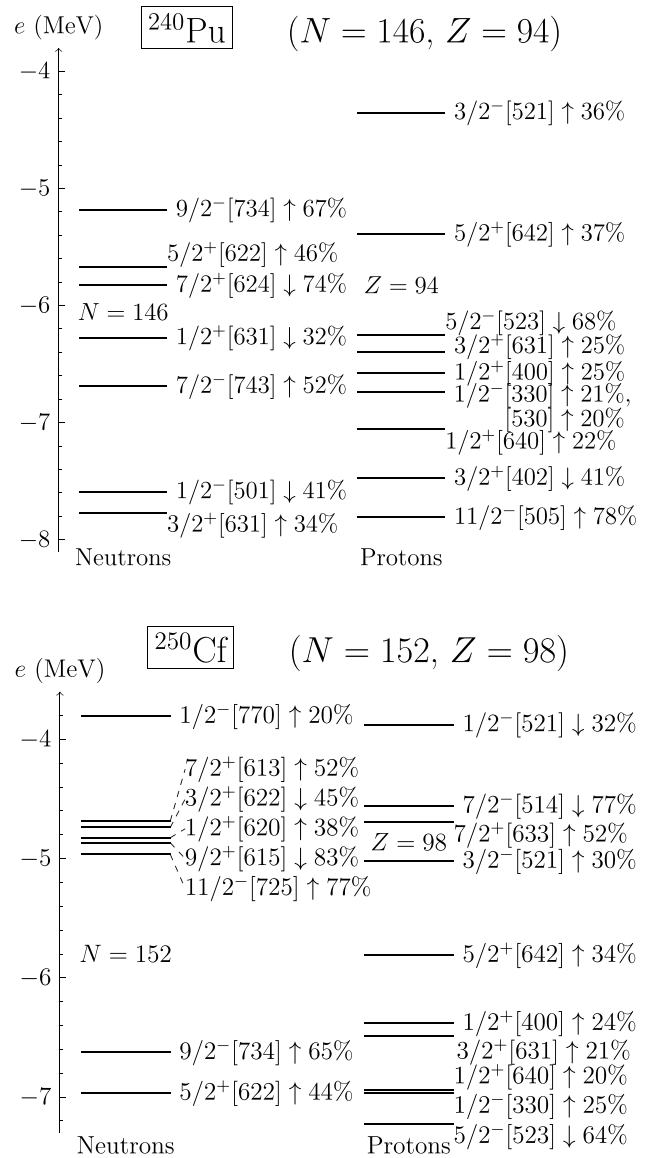
Among the selected Gallagher-Moszkowski doublets in these two isotopes of Pa, the K^π quantum numbers of the calculated lowest-lying state agree with experiment. Moreover, apart from two cases, namely the (0^- , 1^-) and (2^+ , 3^+) doublets, the calculated excitation energies agree very well with experiment, within about 100 keV at most. The largest

FIG. 12. Same as Fig. 4 for the ^{230}Th nucleus.

discrepancy between theory and experiment is obtained for the $(0^-, 1^-)$ doublet with an overestimation of the excitation energies of about 1 MeV in ^{230}Pa and about 250 keV in ^{234}Pa and the $(2^+, 3^+)$ doublet in ^{230}Pa with an overestimation of about 300 to 400 keV. Since the excitation energies of the doublets involving the $1/2^- [530]$ proton single-particle states other than $(2^+, 3^+)$ [e.g., the $(2^-, 3^-)$ Gallagher-Moszkowski doublets in ^{230}Pa] are well reproduced, the above overestimation is essentially caused by the $1/2^+ [631]$ neutron state clearly too far above the neutron Fermi level of ^{230}Th . As this is less so in ^{234}Pa , we can ascribe this to an overestimated $N = 142$ shell gap.

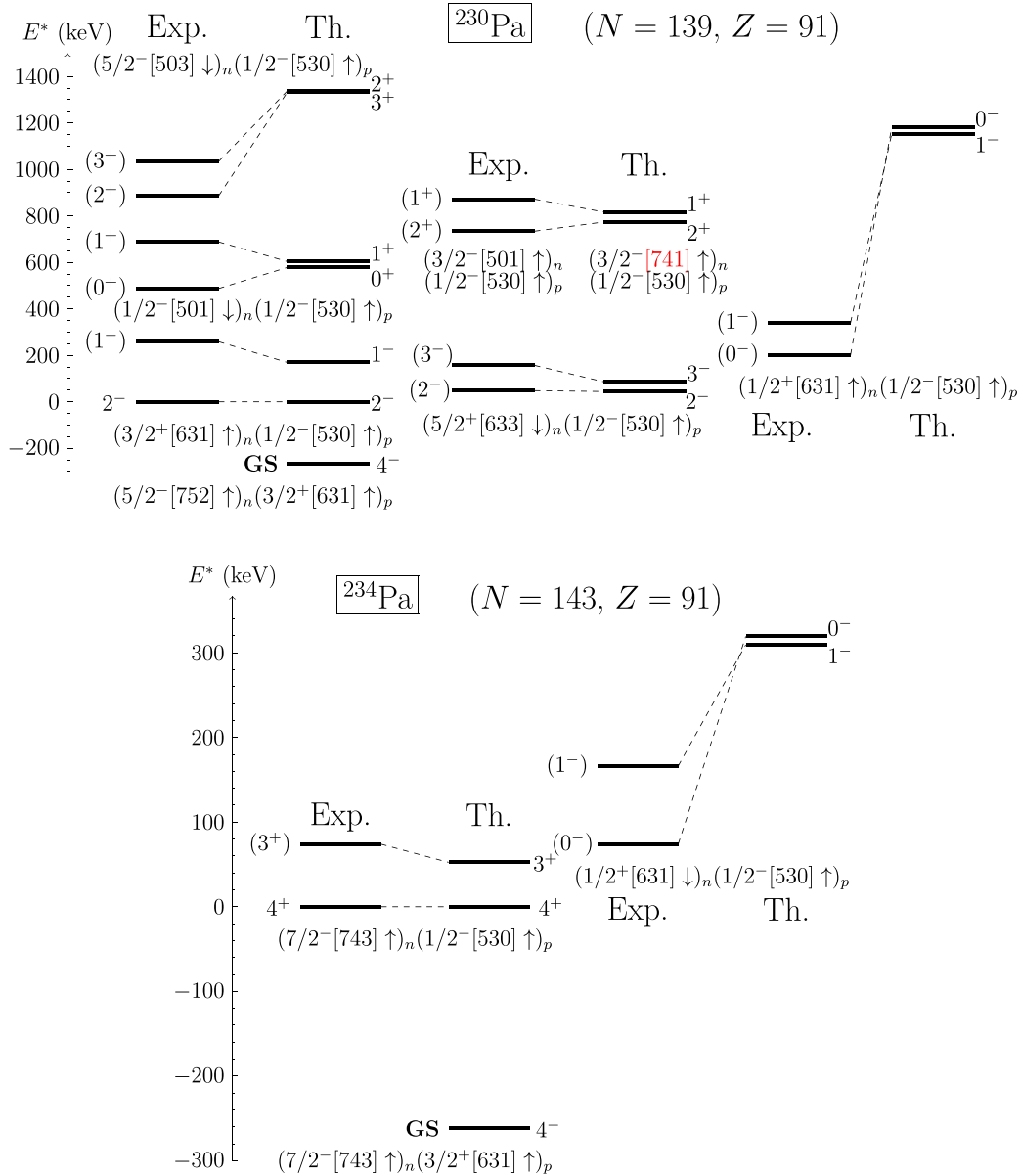
^{238}Np and $^{240,242,244}\text{Am}$ nuclei. Figure 15 shows the spectra of these doubly odd nuclei around $A = 240$. Note that in ^{242}Am the ground state (not reported in Fig. 15) is the 1^- member of the $K^\pi = 0^-$ band, so we have set the excitation energy of the 0^- state to the experimental value (44.092 keV) and placed all the other calculated states in the ^{242}Am spectrum with respect to the calculated $K^\pi = 0^-$ state.

In ^{238}Np we find the experimentally observed $(2^-, 3^-)$ doublet about 200 keV below the $(3^+, 2^+)$ doublet involving the 2^+ experimental ground state. The configurations of these two doublets differ by the proton states $5/2^- [523] \downarrow$ and $5/2^+ [642] \uparrow$, which have the same Ω quantum number but opposite parities, the $1/2^+ [631]$ neutron blocked state being common to these two doublets. As shown by Fig. 13, the $5/2^- [523]$ state is calculated to be of hole character in ^{240}Pu whereas the $5/2^+ [642]$ state is of particle character. This explains why the $(2^-, 3^-)$ doublet lies below the $(3^+, 2^+)$ doublet in ^{238}Np . Therefore these two $\Omega = 5/2$ proton states are inverted in the calculated single-particle spectrum. This

FIG. 13. Same as Fig. 4 for the ^{240}Pu and ^{250}Cf nuclei. In ^{240}Pu , the second largest component of the $1/2^-$ proton state is also given, below the dominant one.

interpretation is supported by the reverse ordering of the $(2^-, 3^-)$ and $(3^+, 2^+)$ doublets, based on the above configurations, observed in ^{242}Am . Despite this inversion of the $5/2^+ [642]$ and $5/2^- [523]$ states in the proton single-particle spectrum, the calculated energy splitting in the above $(2^-, 3^-)$ and $(3^+, 2^+)$ doublets agrees very well with experiment in the nuclei where they are observed, namely ^{238}Np and $^{240,242}\text{Am}$.

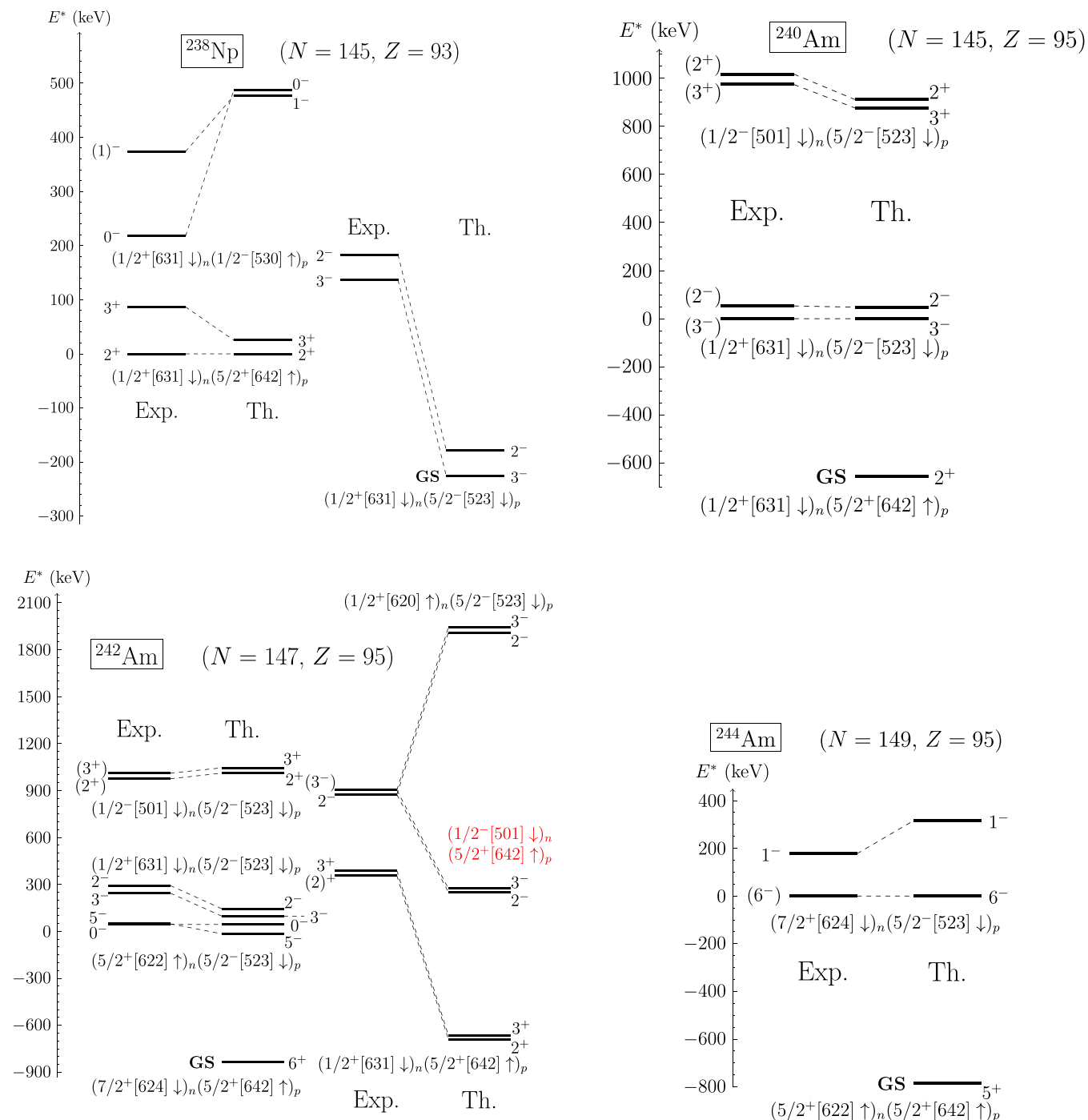
Another large discrepancy is observed in the ^{242}Am for the $(2^-, 3^-)$ doublet based on the $(1/2^+ [620] \uparrow)_n$ ($5/2^- [523] \downarrow$)_p configuration, with an overestimation of the experimental excitation energies of both members of the doublet by about 1 MeV. Because these excitation energies are compared with those of the $(0^-, 5^-)$ doublet which involves the same $5/2^- [523]$ proton state and because the $1/2^+ [620]$ neutron state in the $(2^-, 3^-)$ doublet is calculated to lie

FIG. 14. Same as Fig. 5 for the $^{230,234}\text{Pa}$ nuclei.

above the $N = 152$ shell gap (see the neutron single-particle spectrum of ^{250}Cf in Fig. 13), we deduce that the resulting disagreement is attributable to an overestimation of the $N = 152$ gap. The inversion of the $5/2^+ [642]$ and $5/2^- [523]$ states across the proton Fermi level in a neighboring Pu nucleus makes thus more favorable to form a $(2^-, 3^-)$ doublet with the proton state $5/2^+ [642]$ of particle character and a $1/2^-$ neutron near the Fermi level of ^{240}Pu . As displayed in Fig. 13, the nearest $1/2^-$ neutron state is $1/2^- [501]$, just below the $N = 142$ shell gap. Blocking this neutron state and the $5/2^+ [642]$ proton eventually gives a $(2^-, 3^-)$ doublet with an excitation energy of a little bit less than 300 keV, hence much lower than the one based on the proposed $(1/2^+ [620] \uparrow)_n (5/2^- [523] \downarrow)_p$ configuration. Not surprisingly it is also calculated to lie well below the $(2^+, 3^+)$ doublet based on the $(1/2^- [501] \downarrow)_n (5/2^- [523] \downarrow)_p$, as a consequence of the

inversion of the two $5/2$ proton states. However, it is remarkable that the energy splittings in the $(2^-, 3^-)$ doublets built on $(1/2^- [501] \downarrow)_n (5/2^+ [642] \uparrow)_p$ and $(1/2^+ [620] \uparrow)_n (5/2^- [523] \downarrow)_p$ are virtually the same. Part of the reason could be that both configurations lead to spin antialignment in the 3^- state.

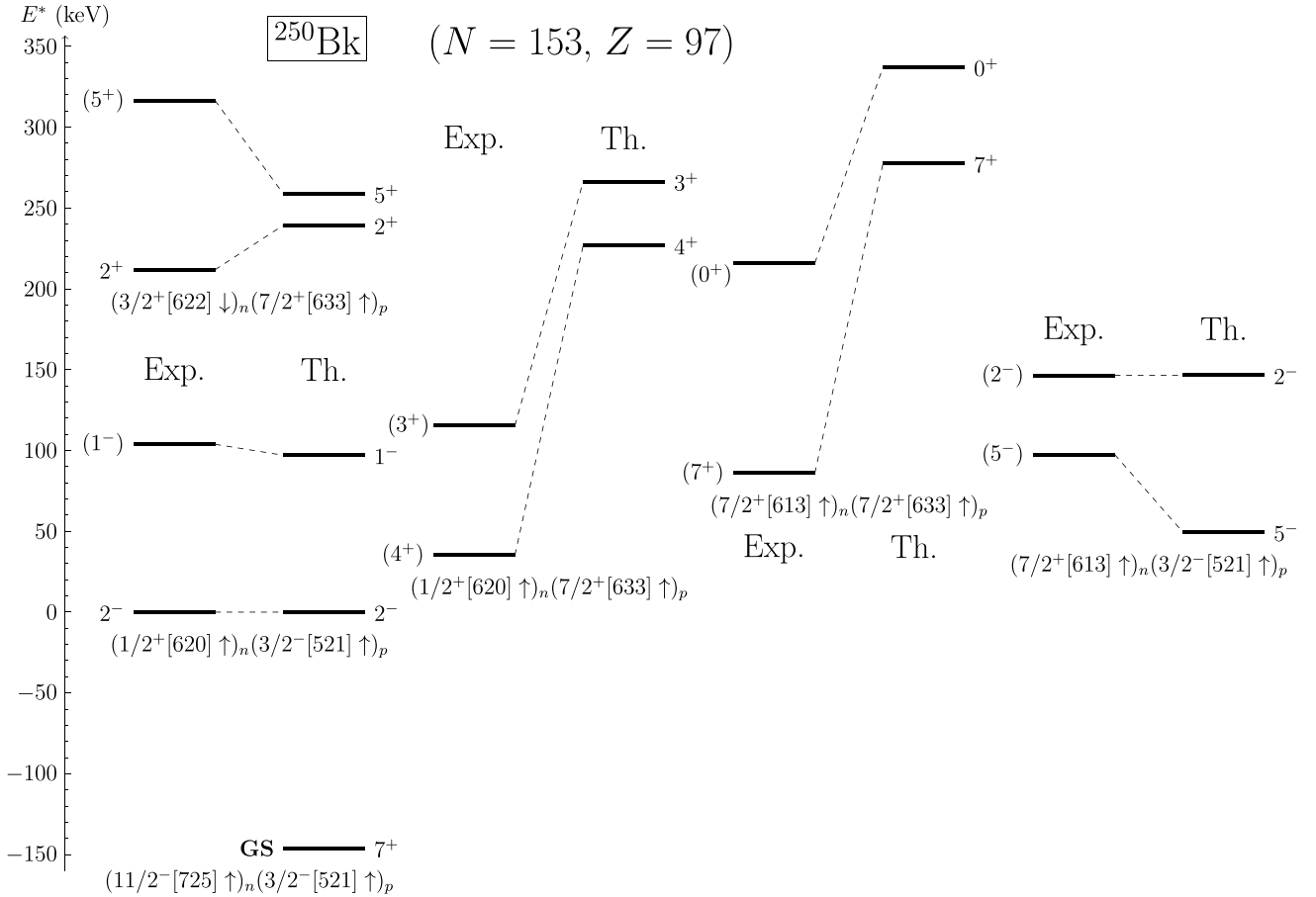
^{250}Bk nucleus. The spectrum of this nucleus is shown in Figure 16, with an energy scale much less compressed than in previous spectra. This nucleus is particularly interesting because it has one more neutron than the “deformed magic number” $N = 152$ so that the unpaired (blocked) neutron state falls into a region of very high level density as one can infer from the neutron single-particle level spectrum of ^{250}Cf in Fig. 13. In contrast the proton level density just below the $Z = 98$ gap in the single-particle spectrum is low. Therefore many configurations can be expected to yield

FIG. 15. Same as Fig. 5 for the ^{238}Np and $^{240,242,244}\text{Am}$ nuclei.

Gallagher-Moszkowski doublets at low excitation energies, so that comparison with experiment will prove to be a demanding test of the model.

The experimentally observed doublets all involve a neutron state just above the $N = 152$ shell gap, namely $1/2^+[620]$, $3/2^+[622]$, and $7/2^+[613]$ (they are among the five levels grouped near $e = -5$ MeV in the single-particle spectrum of ^{250}Cf). On the proton side, the observed doublets involve either the $3/2^- [521]$ state (of hole character in ^{250}Cf) or the

$7/2^+[633]$ state (of particle character in ^{250}Cf). Among these doublets, the lowest lying one includes the ground state 2^- of ^{250}Bk and is interpreted as a $(1/2^+[620] \uparrow)_n (3/2^- [521] \uparrow)_p$ two-quasiparticle configuration. Although Fig. 16 seems to exhibit large discrepancies between theory and experiment for some states, our calculations reproduce extremely well the excited 2^- state among the nine considered excited states and produce the eight other excited states with less than 350 keV excitation energy.

FIG. 16. Same as Fig. 5 for the ^{250}Bk nucleus.

Moreover, the largest discrepancy between the experimental excitation energy and the calculated one is about 200 keV. It occurs in the $(4^+, 3^+)$ and $(7^+, 0^+)$ doublets, whereas in the other doublets the discrepancy is below 80 keV or so, which would look very good at the scale of the previous spectra. The particularly low excitation energies of these doublets make less justified the conclusions that can be drawn about the energy width of the $Z = 98$ gap because beyond mean-field correlations could have an effect of the same order of magnitude as the above discrepancies. However, the energy difference between the (4^+) and (7^+) states being well reproduced, we can deduce that the (small) energy spacing between the $1/2^+[620]$ and $7/2^+[613]$ neutron single-particle states is correct.

IV. GALLAGHER-MOSZKOWSKI ENERGY SPLITTING

We now focus on the energy splitting ΔE_{GM} in Gallagher-Moszkowski doublets studied in the previous section. We recall that it is defined as the difference between the excitation energies of the spin-antialigned and spin-aligned configurations, $\Delta E_{\text{GM}} = E_{\uparrow\downarrow} - E_{\uparrow\uparrow}$, and that it should be positive according to the Gallagher-Moszkowski rule [3]. This quantity strongly depends on the two-quasiparticle configuration on which the doublet is built and is a relative excitation energy, so we expect it to be weakly dependent

of the potential discrepancies between the calculated and measured energy spectra of odd-odd nuclei.

A. Self-consistent blocking

The ΔE_{GM} values resulting from the self-consistent blocking calculations reported in the previous section are displayed in the column “SCB” of Table I.

The first global observation that can be made relates to the sign of the calculated ΔE_{GM} values. For the lighter rare-earth nuclei considered in this work, from ^{154}Eu to ^{172}Tm , the calculated Gallagher-Moszkowski energy splittings are all positive except in four cases. Out of these four exceptions three correspond to a very small value of $|\Delta E_{\text{GM}}| < 3$ keV and one (in ^{158}Tb) is such that $|\Delta E_{\text{GM}}| \approx 25$ keV. One can thus conclude that our calculations are in an overall qualitative agreement with the empirical rule in all five investigated nuclei. More quantitatively this corresponds to an about 80% of agreement with experiment. In contrast, in the other studied rare-earth-and-beyond nuclei, from ^{174}Lu to ^{180}Ta , we find eight cases with $\Delta E_{\text{GM}} \leq 0$ out of 24 experimentally observed doublets in these Lu and Ta nuclei, hence a percentage of agreement of about 66% in this mass region. Finally, in the studied actinides, from ^{230}Pa to ^{250}Bk , the sign of the energy splitting ΔE_{GM} is much better reproduced than in the Lu and Ta doublets, with only four discrepant cases out of a

TABLE I. Energy difference ΔE_{GM} between spin-antialigned and spin-aligned states of Gallagher-Moszkowski doublets. The column labeled “Total” corresponds to $\Delta E_{\text{GM}}^{\text{(pert)}}$ whereas the contributions $\Delta E_{\text{GM}}^{(t_0)}$, $\Delta E_{\text{GM}}^{(t_3)}$, $\Delta E_{\text{GM}}^{(t_1+t_2)}$, and $\Delta E_{\text{GM}}^{(W)}$ defined in Eqs. (3a) to (3d) are reported in the four preceding columns. Experimental data are taken from references quoted in the last column. In ^{178}Ta the ground state is taken to be the 7^- state as in Refs. [28,29] and we use the excitation energy of the 1^+ isomer estimated from systematics 100 keV given by Ref. [29].

Nucleus	Configuration	$(K_{\uparrow}, K_{\downarrow})^{\pi}$	ΔE_{GM} (keV)							SCB	Exp.	Refs.
			Perturb.				Total	SCB	Exp.			
			t_0	t_3	$t_1 + t_2$	W						
^{154}Eu	$(11/2^- [505] \uparrow 93\%)_n(5/2^+ [413] \downarrow 84\%)_p$	$(3, 8)^-$	281.1	-140.1	-135.4	47.3	53.0	21.7	145.3	[32–34]		
^{154}Eu	$(3/2^+ [651] \uparrow 35\%)_n(5/2^+ [413] \downarrow 83\%)_p$	$(1, 4)^+$	117.9	-64.3	-42.2	0.7	12.1	-2.8	131.905			
^{154}Eu	$(3/2^- [521] \uparrow 55\%)_n(5/2^+ [413] \downarrow 83\%)_p$	$(1, 4)^-$	119.4	-41.9	-42.5	0.0	35.0	18.9	152.459			
^{154}Eu	$(3/2^- [521] \uparrow 54\%)_n(3/2^+ [411] \uparrow 58\%)_p$	$(3, 0)^-$	290.4	-155.0	74.5	9.3	219.3	203.8	39.7488			
^{156}Eu	$(5/2^+ [642] \uparrow 53\%)_n(5/2^+ [413] \downarrow 84\%)_p$	$(0, 5)^+$	183.6	-96.1	-75.5	12.6	24.6	-0.8	145.682	[35]		
^{156}Eu	$(3/2^- [521] \uparrow 56\%)_n(5/2^+ [413] \downarrow 83\%)_p$	$(1, 4)^-$	119.4	-42.5	-42.5	0.0	34.5	20.4	127.441			
^{156}Eu	$(5/2^+ [642] \uparrow 53\%)_n(5/2^- [532] \uparrow 60\%)_p$	$(5, 0)^-$	336.5	-154.5	139.4	4.5	325.9	264.6	68.1036			
^{156}Eu	$(3/2^- [521] \uparrow 56\%)_n(5/2^- [532] \uparrow 60\%)_p$	$(4, 1)^+$	123.8	-46.9	45.3	-3.4	118.8	94.6	116.154			
^{158}Tb	$(3/2^- [521] \uparrow 55\%)_n(3/2^+ [411] \uparrow 59\%)_p$	$(3, 0)^-$	299.2	-160.5	74.7	8.5	221.9	207.5	110.3	[25]		
^{158}Tb	$(5/2^+ [642] \uparrow 53\%)_n(3/2^+ [411] \uparrow 59\%)_p$	$(4, 1)^+$	110.0	-46.1	19.2	-4.1	79.1	56.8	123.86			
^{158}Tb	$(11/2^- [505] \uparrow 92\%)_n(3/2^+ [411] \uparrow 60\%)_p$	$(7, 4)^-$	162.4	-64.8	25.3	-12.5	110.4	90.8	107.01			
^{158}Tb	$(3/2^+ [402] \downarrow 74\%)_n(3/2^+ [411] \uparrow 60\%)_p$	$(0, 3)^+$	286.1	-152.6	-75.7	-32.7	25.1	-25.4	181.9			
^{158}Tb	$(1/2^+ [640] \uparrow 25\%)_n(3/2^+ [411] \uparrow 58\%)_p$	$(2, 1)^+$	48.2	-23.4	4.6	4.1	33.5	17.7	60.9			
^{158}Tb	$(3/2^- [521] \uparrow 54\%)_n(7/2^+ [404] \downarrow 87\%)_p$	$(2, 5)^-$	101.2	-39.5	-27.1	10.5	45.1	32.6	108			
^{160}Tb	$(3/2^- [521] \uparrow 55\%)_n(3/2^+ [411] \uparrow 59\%)_p$	$(3, 0)^-$	299.2	-161.7	74.7	8.5	220.7	210.3	79.0925	[36]		
^{160}Tb	$(5/2^- [523] \downarrow 73\%)_n(3/2^+ [411] \uparrow 59\%)_p$	$(1, 4)^-$	141.5	-56.2	-43.3	-16.3	25.7	8.6	193.855			
^{160}Tb	$(5/2^+ [642] \uparrow 52\%)_n(3/2^+ [411] \uparrow 59\%)_p$	$(4, 1)^+$	110.0	-46.7	19.2	-4.1	78.5	54.7	74.6254			
^{160}Tb	$(5/2^+ [642] \uparrow 52\%)_n(5/2^+ [413] \downarrow 83\%)_p$	$(0, 5)^+$	185.8	-99.0	-75.3	11.6	23.1	-2.6	203.371			
^{172}Tm	$(5/2^- [512] \uparrow 73\%)_n(1/2^+ [411] \downarrow 65\%)_p$	$(2, 3)^-$	400.9	-208.0	-80.4	58.6	171.1	92.9	62.529	[37]		
^{172}Tm	$(1/2^- [521] \downarrow 54\%)_n(1/2^+ [411] \downarrow 64\%)_p$	$(1, 0)^-$	242.0	-122.7	45.6	17.0	181.9	171.1	68.108			
^{172}Tm	$(5/2^- [512] \uparrow 73\%)_n(7/2^- [523] \uparrow 77\%)_p$	$(6, 1)^+$	143.2	-57.2	51.6	-6.2	131.4	106.7	133.862	[38]		
^{174}Lu	$(5/2^- [512] \uparrow 72\%)_n(7/2^+ [404] \downarrow 92\%)_p$	$(1, 6)^-$	139.0	-56.7	-55.7	-2.5	24.1	9.1	170.83	[39]		
^{174}Lu	$(7/2^+ [633] \uparrow 71\%)_n(7/2^+ [404] \downarrow 92\%)_p$	$(0, 7)^+$	197.3	-106.6	-99.5	6.2	-2.6	-29.3	150.242			
^{174}Lu	$(1/2^- [521] \downarrow 51\%)_n(7/2^+ [404] \downarrow 92\%)_p$	$(4, 3)^-$	86.6	-37.4	12.8	8.0	70.0	55.1	67.697			
^{174}Lu	$(5/2^- [512] \uparrow 72\%)_n(9/2^- [514] \uparrow 87\%)_p$	$(7, 2)^+$	257.5	-99.5	67.4	-4.6	220.8	151.3	104.1			
^{176}Lu	$(7/2^- [514] \downarrow 86\%)_n(7/2^+ [404] \downarrow 91\%)_p$	$(7, 0)^-$	305.6	-163.1	180.5	10.7	333.7	314.6	236.908	[40]		
^{176}Lu	$(7/2^- [514] \downarrow 85\%)_n(9/2^- [514] \uparrow 86\%)_p$	$(1, 8)^+$	487.9	-251.9	-246.8	8.9	-1.9	-145.4	293.482			
^{176}Lu	$(9/2^+ [624] \uparrow 83\%)_n(7/2^+ [404] \downarrow 91\%)_p$	$(1, 8)^+$	269.0	-141.7	-137.8	19.9	9.3	-39.7	86.0468			
^{176}Lu	$(7/2^- [514] \downarrow 86\%)_n(5/2^+ [402] \uparrow 69\%)_p$	$(1, 6)^-$	159.1	-69.0	-61.8	-11.6	16.6	4.6	177.357			
^{176}Lu	$(5/2^- [512] \uparrow 70\%)_n(7/2^+ [404] \downarrow 91\%)_p$	$(1, 6)^-$	139.0	-57.7	-55.7	-2.5	23.1	7.7	127.911			
^{176}Lu	$(7/2^- [514] \downarrow 86\%)_n(1/2^- [541] \downarrow 33\%)_p$	$(4, 3)^+$	42.7	-23.3	18.1	6.3	43.8	37.0	99.162			
^{176}Lu	$(1/2^- [510] \uparrow 65\%)_n(7/2^+ [404] \downarrow 91\%)_p$	$(3, 4)^-$	117.6	-49.1	-2.5	2.8	68.9	49.3	129.779			
^{176}Lu	$(7/2^- [514] \downarrow 87\%)_n(1/2^+ [411] \downarrow 61\%)_p$	$(4, 3)^-$	267.5	-123.0	34.3	8.1	186.9	130.5	120.506			
^{176}Lu	$(9/2^+ [624] \uparrow 83\%)_n(5/2^+ [402] \uparrow 70\%)_p$	$(7, 2)^+$	141.8	-59.7	38.1	-3.0	117.1	86.9	132.323			
^{176}Lu	$(3/2^- [512] \downarrow 71\%)_n(7/2^+ [404] \downarrow 91\%)_p$	$(5, 2)^-$	139.2	-58.5	42.6	2.3	125.5	90.9	194.861			
^{176}Lu	$(1/2^- [521] \downarrow 49\%)_n(7/2^+ [404] \downarrow 91\%)_p$	$(4, 3)^-$	86.6	-37.9	12.8	8.0	69.5	52.5	49.642			
^{176}Lu	$(7/2^- [514] \downarrow 86\%)_n(7/2^- [523] \uparrow 76\%)_p$	$(0, 7)^+$	292.8	-152.7	-140.3	15.0	14.8	-41.4	217.5			
^{178}Lu	$(9/2^+ [624] \uparrow 82\%)_n(7/2^+ [404] \downarrow 91\%)_p$	$(1, 8)^+$	264.8	-139.0	-134.6	20.8	12.0	-38.3	187	[28,41]		
^{178}Ta	$(7/2^- [514] \downarrow 86\%)_n(5/2^+ [402] \uparrow 67\%)_p$	$(1, 6)^-$	159.1	-69.6	-60.8	-10.9	17.8	6.2	188.1	[28,42]		
^{178}Ta	$(7/2^- [514] \downarrow 86\%)_n(9/2^- [514] \uparrow 86\%)_p$	$(1, 8)^+$	478.3	-247.9	-237.9	10.5	3.0	-141.0	100	[29]		
^{180}Ta	$(9/2^+ [624] \uparrow 81\%)_n(7/2^+ [404] \downarrow 90\%)_p$	$(1, 8)^+$	264.8	-140.4	-134.6	20.8	10.6	-36.9	177.87	[43]		
^{180}Ta	$(9/2^+ [624] \uparrow 82\%)_n(9/2^- [514] \uparrow 85\%)_p$	$(9, 0)^-$	310.9	-151.9	173.5	-10.8	321.7	264.1	30.58			

TABLE I. (*Continued.*)

Nucleus	Configuration	$(K_{\uparrow\uparrow}, K_{\uparrow\downarrow})^\pi$	ΔE_{GM} (keV)								Refs.
			Perturb.				Total	SCB	Exp.		
			t_0	t_3	$t_1 + t_2$	W					
^{180}Ta	$(7/2^- [514] \downarrow 86\%)_n (9/2^- [514] \uparrow 85\%)_p$	$(1, 8)^+$	478.3	-251.0	-237.9	10.5	-0.2	-138.4	195.57		
^{180}Ta	$(9/2^+ [624] \uparrow 83\%)_n (5/2^+ [402] \uparrow 66\%)_p$	$(7, 2)^+$	138.6	-59.4	37.3	-3.2	113.3	80.9	202.49		
^{180}Ta	$(5/2^- [512] \uparrow 68\%)_n (7/2^+ [404] \downarrow 90\%)_p$	$(1, 6)^-$	140.5	-60.6	-55.3	-4.3	20.3	3.7	151.43		
^{230}Pa	$(5/2^- [503] \downarrow 52\%)_n (1/2^- [530] \uparrow 24\%)_p$	$(2, 3)^+$	54.3	-23.8	-4.1	-16.7	9.7	5.4	148	[31,44]	
^{230}Pa	$(3/2^+ [631] \uparrow 33\%)_n (1/2^- [530] \uparrow 24\%)_p$	$(2, 1)^-$	358.2	-204.0	5.1	71.1	230.3	169.7	259		
^{230}Pa	$(5/2^+ [633] \downarrow 57\%)_n (1/2^- [530] \uparrow 24\%)_p$	$(2, 3)^-$	125.0	-57.6	-4.0	1.0	64.4	42.4	109		
^{230}Pa	$(1/2^+ [631] \downarrow 29\%)_n (1/2^- [530] \uparrow 24\%)_p$	$(0, 1)^-$	214.5	-111.7	-3.3	-59.9	39.5	-27.9	139		
^{230}Pa	$(1/2^- [501] \downarrow 37\%)_n (1/2^- [530] \uparrow 24\%)_p$	$(0, 1)^+$	105.8	-59.1	-2.0	-7.1	37.6	25.5	201		
^{230}Pa	$(3/2^- [741] \uparrow 29\%)_n (1/2^- [530] \uparrow 21\%)_p$	$(2, 1)^+$	122.6	-47.4	3.1	3.6	81.8	43.4	138		
^{234}Pa	$(7/2^- [743] \uparrow 52\%)_n (1/2^- [530] \uparrow 22\%)_p$	$(4, 3)^+$	149.9	-61.1	2.6	-2.3	89.1	52.4	73.92	[45,46]	
^{234}Pa	$(1/2^+ [631] \downarrow 30\%)_n (1/2^- [530] \uparrow 22\%)_p$	$(0, 1)^-$	225.3	-120.9	-3.2	-60.1	41.1	-10.0	92.38	[45-47]	
^{238}Np	$(1/2^+ [631] \downarrow 33\%)_n (5/2^+ [642] \uparrow 38\%)_p$	$(2, 3)^+$	110.4	-46.0	-17.9	2.5	49.0	25.2	86.6738	[48]	
^{238}Np	$(1/2^+ [631] \downarrow 33\%)_n (5/2^- [523] \downarrow 69\%)_p$	$(3, 2)^-$	89.5	-37.1	16.6	1.2	70.3	47.8	46.8325		
^{238}Np	$(1/2^+ [631] \downarrow 32\%)_n (1/2^- [530] \uparrow 21\%)_p$	$(0, 1)^-$	252.6	-135.5	-3.1	-59.1	55.0	-10.7	155.735		
^{240}Am	$(1/2^+ [631] \downarrow 34\%)_n (5/2^- [523] \downarrow 69\%)_p$	$(3, 2)^-$	89.5	-37.6	16.7	1.2	69.8	47.9	53	[49]	
^{240}Am	$(1/2^- [501] \downarrow 43\%)_n (5/2^- [523] \downarrow 69\%)_p$	$(3, 2)^+$	66.1	-31.7	7.7	-1.5	40.6	34.9	43		
^{242}Am	$(5/2^+ [622] \uparrow 46\%)_n (5/2^- [523] \downarrow 68\%)_p$	$(0, 5)^-$	158.7	-75.8	-60.3	-32.8	-10.2	-59.7	4.508	[50]	
^{242}Am	$(1/2^+ [631] \downarrow 33\%)_n (5/2^- [523] \downarrow 68\%)_p$	$(3, 2)^-$	90.0	-37.9	16.3	1.4	69.8	47.2	48.48		
^{242}Am	$(1/2^+ [631] \downarrow 32\%)_n (5/2^+ [642] \uparrow 36\%)_p$	$(2, 3)^+$	111.2	-46.6	-17.5	2.0	49.1	24.7	32.49		
^{242}Am	$(1/2^+ [620] \uparrow 37\%)_n (5/2^- [523] \downarrow 69\%)_p$	$(2, 3)^-$	142.9	-70.5	-2.8	-1.9	67.7	32.9	28.42		
^{242}Am	$(1/2^- [501] \downarrow 43\%)_n (5/2^+ [642] \uparrow 36\%)_p$	$(2, 3)^-$	52.0	-27.1	-5.2	1.4	21.0	21.9	28.42		
^{242}Am	$(1/2^- [501] \downarrow 43\%)_n (5/2^- [523] \downarrow 68\%)_p$	$(3, 2)^+$	65.5	-31.8	7.8	-1.6	39.9	33.6	-36		
^{244}Am	$(7/2^+ [624] \downarrow 75\%)_n (5/2^- [523] \downarrow 68\%)_p$	$(6, 1)^-$	389.2	-219.3	145.5	33.5	348.9	315.5	177.2	[51,52]	
^{250}Bk	$(1/2^+ [620] \uparrow 38\%)_n (3/2^- [521] \uparrow 30\%)_p$	$(2, 1)^-$	204.2	-105.6	4.4	33.8	136.7	97.1	103.83	[53]	
^{250}Bk	$(1/2^+ [620] \uparrow 38\%)_n (7/2^+ [633] \uparrow 52\%)_p$	$(4, 3)^+$	91.2	-38.2	2.6	-0.3	55.3	39.6	80.06		
^{250}Bk	$(7/2^+ [613] \uparrow 51\%)_n (7/2^+ [633] \uparrow 53\%)_p$	$(7, 0)^+$	82.5	-36.7	34.0	-4.3	75.5	59.6	129.94		
^{250}Bk	$(7/2^+ [613] \uparrow 51\%)_n (3/2^- [521] \uparrow 30\%)_p$	$(5, 2)^-$	109.1	-55.7	36.0	14.0	103.4	97.1	48.94		
^{250}Bk	$(3/2^+ [622] \downarrow 45\%)_n (7/2^+ [633] \uparrow 52\%)_p$	$(2, 5)^+$	111.4	-47.2	-30.1	1.6	35.7	19.5	104.64		

total of 25 experimentally observed doublets (84% of agreement), slightly better than in the lighter studied rare-earth nuclei.

Another global observation about the calculated energy splittings relates to their amplitude. In the majority of cases we obtain ΔE_{GM} between 0 and 100 keV, but it can reach 300 keV in doublets with a large difference in K values. The cases breaking the Gallagher-Moszkowski rule correspond to $|\Delta E_{GM}| \lesssim 50$ keV except for one doublet ($1^+, 8^+$) in three nuclei (^{176}Lu , $^{178,180}\text{Ta}$) for which $\Delta E_{GM} \approx -140$ keV.

To better understand these observations and try to unravel the mechanism of energy splitting in Gallagher-Moszkowski doublets within the Skyrme energy-density functional framework, we consider a perturbative approach to blocking.

B. Perturbative blocking

Perturbative blocking corresponds to performing one Hartree-Fock-BCS iteration with blocking on top of the

converged ground-state solution of a neighboring even-even nucleus (called a ‘‘core’’). Therefore there is some arbitrariness in the choice of this even-even core among four possible neighboring even-even nuclei. Because we selected the studied odd-odd nuclei as being neighbors of chosen even-even ones, as shown in Figs. 2 and 3, we decide to choose the cores among these doubly even nuclei. Table II lists the retained even-even cores.

The observable we are studying is essentially dependent on the neutron and proton single-particle wave functions involved in the blocked configuration. Indeed we find that, assuming perturbative blocking,

$$\Delta E_{GM} = \langle n\bar{p} | \widehat{V}_{Sk} | \widetilde{n\bar{p}} \rangle, \quad (1)$$

where \widehat{V}_{Sk} is the Skyrme effective potential (including the density-dependent term with the nucleon density of the core), $|n\rangle$ is the blocked neutron single-particle state, $|\bar{p}\rangle$ is the time reversal of the proton blocked state and $|\widetilde{n\bar{p}}\rangle = |n\bar{p}\rangle - |\bar{p}n\rangle$.

TABLE II. List of the retained even-even core for each studied odd-odd nucleus.

Odd-odd nuclei	Even-even core
$^{154,156}\text{Eu}$	^{156}Gd
$^{158,160}\text{Tb}$	^{158}Gd
$^{172}\text{Tm}, ^{174,176}\text{Lu}$	^{174}Yb
$^{178}\text{Lu}, ^{178,180}\text{Ta}$	^{178}Hf
^{230}Pa	^{230}Th
^{234}Pa	^{232}Th
^{240}Am	^{240}Pu
$^{242,244}\text{Am}$	^{242}Pu
^{250}Bk	^{250}Cf

Therefore we expect that the dependence of the perturbatively calculated ΔE_{GM} on the core is weak.

First we check whether calculations with perturbative blocking on top of the mean field of a neighboring even-even nucleus lead to an energy splitting, denoted by $\Delta E_{\text{GM}}^{(\text{pert})}$, comparable to the one obtained with self-consistent blocking, denoted by $\Delta E_{\text{GM}}^{(\text{SCB})}$. Table I displays the ΔE_{GM} values obtained with perturbative (in the column labeled “Total”) and self-consistent blocking (in the column labeled “SCB”) for all the 70 Gallagher-Moszkowski doublets considered in the present work, and Fig. 17 shows the correlation plot of $\Delta E_{\text{GM}}^{(\text{pert})}$ and $\Delta E_{\text{GM}}^{(\text{SCB})}$ for all these doublets as well as the linear regression equation and correlation coefficient. The latter is found to be almost equal to 1, whereas three outliers are

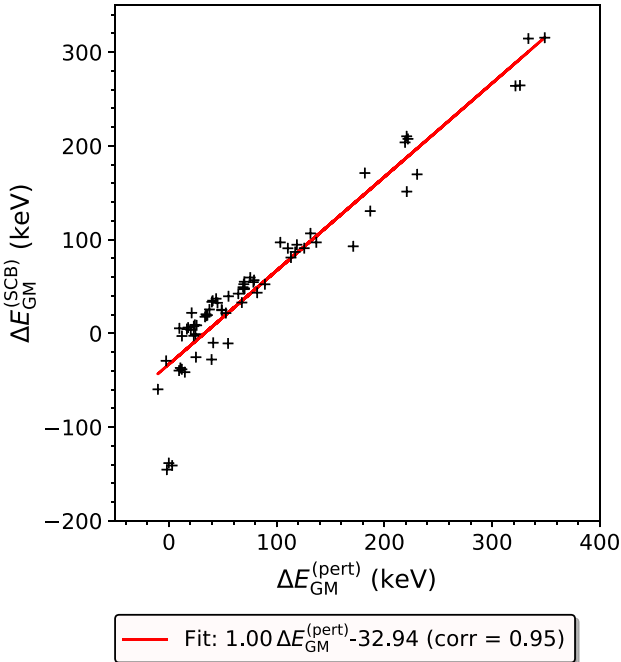


FIG. 17. Correlation plot of $\Delta E_{\text{GM}}^{(\text{SCB})}$ as a function of $\Delta E_{\text{GM}}^{(\text{pert})}$ for the 70 Gallagher-Moszkowski doublets considered in the present work. The correlation coefficient of the linear regression is denoted by “corr”.

clearly visible in the plot. These outliers correspond precisely to the $(1^+, 8^+)$ doublet in the three aforementioned nuclei ^{176}Lu and $^{178,180}\text{Ta}$. Moreover the intercept in the equation of linear regression is calculated to be about -33 keV, which means that the ΔE_{GM} value calculated with self-consistent blocking tends to be a bit smaller than the one obtained with perturbative blocking. Thus in most cases $\Delta E_{\text{GM}}^{(\text{SCB})}$ and $\Delta E_{\text{GM}}^{(\text{pert})}$ have the same sign and order of magnitude, and the discrepancies occur in doublets for which the splitting is small (below a few tens of keV). This statistic analysis establishes the relevance of perturbative calculations to investigate the mechanism of Gallagher-Moszkowski splitting. This will be done in the next subsection through an analysis of the contributions to ΔE_{GM} from the various terms of the Skyrme energy-density functional.

C. Mechanism of the Gallagher-Moszkowski splitting

We now address the mechanism by which the Gallagher-Moszkowski energy splitting ΔE_{GM} occurs in the perturbative-blocking framework. In the Appendix we derive the following expressions of the contributions of the Skyrme EDF to ΔE_{GM} :

$$\Delta E_{\text{GM}}^{(\text{pert})} = \Delta E_{\text{GM}}^{(t_0)} + \Delta E_{\text{GM}}^{(t_3)} + \Delta E_{\text{GM}}^{(t_1+t_2)} + \Delta E_{\text{GM}}^{(W)}, \quad (2)$$

where

$$\Delta E_{\text{GM}}^{(t_0)} = -t_0 x_0 \int d^3\mathbf{r} \mathbf{s}_n \cdot \mathbf{s}_p, \quad (3a)$$

$$\Delta E_{\text{GM}}^{(t_3)} = -\frac{t_3}{6} \int d^3\mathbf{r} \rho^\alpha \mathbf{s}_n \cdot \mathbf{s}_p, \quad (3b)$$

$$\Delta E_{\text{GM}}^{(t_1+t_2)} = (t_1 + t_2) \int d^3\mathbf{r} \mathbf{j}_n \cdot \mathbf{j}_p, \quad (3c)$$

$$\Delta E_{\text{GM}}^{(W)} = W \int d^3\mathbf{r} (\mathbf{s}_n \cdot \nabla \times \mathbf{j}_p + \mathbf{s}_p \cdot \nabla \times \mathbf{j}_n). \quad (3d)$$

By definition \mathbf{s}_n and \mathbf{s}_p are the neutron and proton local spin densities of the neutron-spin-up–proton-spin-up configuration (which is thus spin aligned). Similarly \mathbf{j}_n and \mathbf{j}_p are the neutron and proton local current densities in this configuration. Therefore the central $\Delta E_{\text{GM}}^{(t_0)}$ and density-dependent $\Delta E_{\text{GM}}^{(t_3)}$ zero-range contributions have the signs of $-t_0 x_0$ and $-t_3$, respectively. According to the values of the SIII parameters, one always has $\Delta E_{\text{GM}}^{(t_0)} > 0$ and $\Delta E_{\text{GM}}^{(t_3)} < 0$. The signs of $\Delta E_{\text{GM}}^{(t_1+t_2)}$ and $\Delta E_{\text{GM}}^{(W)}$, in which $t_1 + t_2 > 0$ and $W > 0$, depend, in contrast, on the spin and orbital contents of the blocked states.

The numerical results for the various contributions to ΔE_{GM} in the perturbative-blocking calculations are displayed in Table I, and are compared with the Gallagher-Moszkowski energy splittings obtained with self-consistent blocking. Several systematic trends in perturbative results emerge from the large number of considered doublets:

- (i) $\Delta E_{\text{GM}}^{(t_0)}$ and $\Delta E_{\text{GM}}^{(t_3)}$ are the largest two contributions in absolute value and are related by $\Delta E_{\text{GM}}^{(t_0)} \approx -2 \Delta E_{\text{GM}}^{(t_3)}$, so that the sum of these two contributions is always positive, of the order of $\Delta E_{\text{GM}}^{(t_0)} + \Delta E_{\text{GM}}^{(t_3)} \approx 50$ to 150 keV.

- (ii) The $\Delta E_{\text{GM}}^{(t_1+t_2)}$ contribution is positive whenever the spin-antialigned configuration corresponds to the smaller of the two K values; in other words, when the lower-lying configuration has the larger K value.
- (iii) The $\Delta E_{\text{GM}}^{(W)}$ contribution is small (less than 25 keV in absolute value) in most configurations, with ten exceptions only for which $|\Delta E_{\text{GM}}^{(W)}|$ ranges from about 35 to 70 keV.

The first two points can be substantiated by the correlation plots of Fig. 18.

The main conclusion from these observations is that the Gallagher-Moszkowski rule is always satisfied in doublets for which the spin-aligned configuration corresponds to the larger K value. This is so because the $t_1 + t_2$ (central gradient) positive contribution adds up to the zero-range contributions, and is not counterbalanced by the too small spin-orbit contribution.

It is possible to go further in the analysis of the contributions to ΔE_{GM} of each term of the Skyrme effective potential if we approximate the neutron spin-up state $|n\rangle$ and proton spin-up state $|p\rangle$ of the corresponding blocked levels (see their definition in the Appendix) by the dominant axially deformed harmonic-oscillator basis state characterized by the Nilsson quantum numbers N_q , $n_{z,q}$, Λ_q , and Σ_q . Under this approximation we establish in the Appendix that

- (i) $\Delta E_{\text{GM}}^{(t_0)}$ and $\Delta E_{\text{GM}}^{(t_3)}$ are respectively proportional to and of the sign of $-t_0 x_0 \Sigma_n \Sigma_p$ and $-\frac{t_3}{6} \Sigma_n \Sigma_p$;
- (ii) $\Delta E_{\text{GM}}^{(t_1+t_2)}$ is proportional to and of the sign of $(t_1 + t_2) \Lambda_n \Lambda_p$;
- (iii) $\Delta E_{\text{GM}}^{(W)}$ is proportional to and of the sign of $W(\Lambda_n - \Lambda_p) I_{pn}$, where I_{pn} is an integral over \mathbb{R}_+ involving products of generalized Laguerre polynomials and their first derivatives defined by Eq. (A24b).

Because $x_0 > 0$ and the t_0 term of the Skyrme effective potential is the dominant and attractive term, it always tends to satisfy the Gallagher-Moszkowski rule. The density-dependent term being repulsive, it always tends to counterbalance the $\Delta E_{\text{GM}}^{(t_0)}$ term as already noticed by Robledo, Bernard, and Bertsch within the Gogny EDF [10].

Moreover $K_{\uparrow\uparrow} = \Lambda_n + \Lambda_p + 1$ while $K_{\uparrow\downarrow} = \Lambda_n - \Lambda_p$. If Λ_n and Λ_p have the same sign, then $|K_{\uparrow\downarrow}| < |K_{\uparrow\uparrow}|$ and $\Delta E_{\text{GM}}^{(t_1+t_2)} > 0$. In other words, the sign of $\Delta E_{\text{GM}}^{(t_1+t_2)}$ is the sign of $\Sigma_{k_n} \Sigma_{k_p}$, where k_n and k_p are such that $\Omega_{k_n} > 0$ and $\Omega_{k_p} > 0$. This explains the above conclusion that our calculations comply with the Gallagher-Moszkowski rule in doublets for which the larger $|K|$ value occurs in the spin-aligned configuration. In addition, this explains why $\Delta E_{\text{GM}}^{(t_1+t_2)}$ is very small in absolute value (a few keV) for doublets involving blocked states with $\Omega = 1/2$ and large for doublets in which Ω_n and Ω_p are large. The magnitude of $\Delta E_{\text{GM}}^{(t_1+t_2)}$ also depends on the overlap of neutron and proton wave functions. Because of the large Λ_q values involved and because neutrons and protons spatial wave functions are the same in the $(7/2^- [514] \downarrow)_n (9/2^- [514] \uparrow)_p$ configuration, the energy splitting in the $(1, 8)^+$ doublet is thus negative and especially

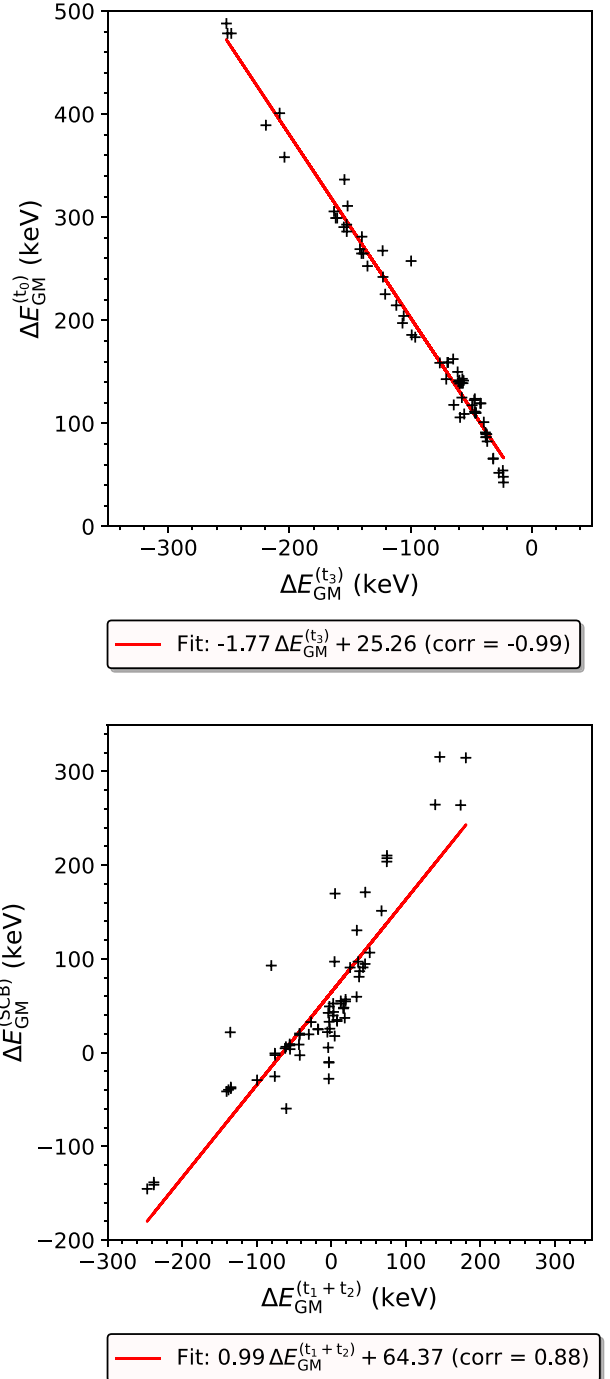


FIG. 18. Same as Fig. 17 for the correlation between $\Delta E_{\text{GM}}^{(t_0)}$ and $\Delta E_{\text{GM}}^{(t_3)}$ (upper panel), and between $\Delta E_{\text{GM}}^{(t_1+t_2)}$ and $\Delta E_{\text{GM}}^{(\text{SCB})}$ (lower panel).

large in absolute value. It amounts to $\Delta E_{\text{GM}}^{(t_1+t_2)} \approx -240$ keV in ^{176}Lu and $^{178,180}\text{Ta}$ nuclei.

Finally, as shown in the Appendix, the spin-orbit contribution $\Delta E_{\text{GM}}^{(W)}$ is difficult to analyze because it strongly depends on the nodal and azimuthal structure of the blocked neutron and proton wave functions. Its sign cannot be simply related to the sign of $\Lambda_n - \Lambda_p$ [see Eq. (A27)], so we do not comment on it further.

V. CONCLUSIONS AND PERSPECTIVES

Within the Skyrme energy-density functional approach, including BCS pairing correlations with self-consistent blocking, we calculate the total energy of 70 Gallagher-Moszkowski doublets of bandheads in rare-earth nuclei around mass numbers $A \approx 156$ and 176 as well as in actinide nuclei around mass numbers $A \approx 230$, 240 and 250. Each bandhead state is described as a one-neutron, one-proton blocked configuration, and axial and intrinsic parity symmetries are assumed. We use the SIII Skyrme parametrization in the particle-hole channel and the seniority pairing interaction. The strengths of the latter interaction for neutrons and for protons are adjusted using the procedure described in Ref. [20] and successfully applied in two-quasiparticle K isomers of actinides in Ref. [13].

First we analyze the bandhead spectra of ten rare-earth and seven actinide odd-odd nuclei by comparison with experimental data. To determine the level scheme of these nuclei from the total energies calculated for each bandhead state, we calculate the excitation energy of a given bandhead state with respect to the experimental lowest-lying bandhead state. All calculated doublets but two are obtained with a two-quasiparticle configuration identical with the one proposed in the literature to interpret the experimental data. The two exceptions are the $(2^+, 1^+)$ doublet of ^{158}Tb with a calculated configuration $(1/2^+[400])_n (3/2^+[411])_p$ instead of $(1/2^+[620])_n (3/2^+[411])_p$, and the $(2^+, 1^+)$ doublet of ^{230}Pa with a calculated configuration $(3/2^-[741])_n (1/2^-[530])_p$ instead of $(3/2^-[501])_n (1/2^-[530])_p$. Moreover the typical discrepancy between the calculated and experimental excitation energies is of the order of 100 to 200 keV, which shows the overall relevance of the calculated single-particle spectra. However there are a few exceptions with large discrepancies which are interpreted by misplaced single-particle states. These occur in particular, but not only, around an exceeding shell gap, such as the $N = 142$ and $N = 152$ gaps in actinides. Also an inversion of $5/2^+$ and $5/2^-$ proton states is observed across the $Z = 94$ gap.

Then we focus on the energy difference ΔE_{GM} between the two members of a Gallagher-Moszkowski doublet and address the mechanism in the Skyrme-EDF framework by which the Gallagher-Moszkowski rule operates. To do so, we first establish the relevance of a study based on calculations with perturbative blocking as compared to self-consistent blocking and then analyze the contributions to ΔE_{GM} from the time-odd part of the Skyrme SIII energy-density functional, namely the central zero-range ΔE_{t_0} term, the central gradient $\Delta E_{\text{GM}}^{(t_1+t_2)}$ term, the central zero-range density-dependent $\Delta E_{\text{GM}}^{(t_3)}$ term, and the zero-range spin-orbit $\Delta E_{\text{GM}}^{(W)}$ term. Given the signs of the involved SIII parameters, we show that the Gallagher-Moszkowski rule is always satisfied in doublets for which the spin-aligned configuration corresponds to the larger K value. This is so because the $\Delta E_{\text{GM}}^{(t_1+t_2)}$ contribution is positive in that case and adds up to the zero-range contributions, and is not counterbalanced by the too small spin-orbit contribution. More precisely, we find that $\Delta E_{\text{GM}}^{(t_1)}$ and $\Delta E_{\text{GM}}^{(t_3)}$ are the largest two contributions in absolute value and are

approximately related by $\Delta E_{\text{GM}}^{(t_1)} \approx 2 \Delta E_{\text{GM}}^{(t_3)}$, so that the sum of these two contributions is always positive, of the order of $\Delta E_{\text{GM}}^{(t_1)} + \Delta E_{\text{GM}}^{(t_3)} \approx 50$ to 150 keV. They can be counterbalanced, and sometimes exceeded in absolute value, by the $\Delta E_{\text{GM}}^{(t_1+t_2)}$ contribution only when the spin-aligned member of a doublet corresponds to the lower of the two K values. This mechanism can be anticipated from the dominant Nilsson quantum numbers of the two-quasiparticle configuration of the doublet, when the involved single-particle wave functions are not too much fragmented in the cylindrical harmonic-oscillator basis. If $\Omega_q [N_q n_{z,q} \Lambda_q]$ denote the Nilsson quantum numbers of the dominant contribution to the charge state q , with $\Omega_q > 0$ by definition, then cases likely to break the Gallagher-Moszkowski rule are such that (i) $\Sigma_n \Sigma_p < 0$, where $\Sigma_q = \Omega_q - \Lambda_q$ is the spin projection on the symmetry axis, and (ii) $\Lambda_n \Lambda_p$ is large (this product is always positive or vanishing by definition of Ω_q).

While the above conclusions are derived from the Skyrme SIII parametrization, a similar study using other parametrizations could be attempted to highlight the interplay between the various terms entering the Skyrme EDF. Indeed, in the above perturbative approach, the contributions to ΔE_{GM} arise from the time-odd terms of the Skyrme EDF and are proportional to combinations of the Skyrme parameters for fixed local densities. Moreover we recall that the $\mathbf{s} \cdot \mathbf{T}$ terms, involving the spin-kinetic \mathbf{T} local density in the notation of Ref. [54], the $\sum_{\mu,\nu} J_{\mu\nu}^2$ terms, involving the spin-current $J_{\mu\nu}$ local density, and the $\mathbf{s} \cdot \Delta \mathbf{s}$ terms are neglected in our so-called “minimal” scheme (as explained in Refs. [17,19]). Therefore different Skyrme parametrizations might yield different competition mechanisms between the time-odd terms. A comparative study of various Skyrme energy-density functionals would thus allow to potentially reveal general features of the Gallagher-Moszkowski energy splitting with the Skyrme-EDF approach. It is worth mentioning that a similar detailed work, pushing further the analysis made by Robledo, Bernard, and Bertsch [10], is in principle possible for Gogny-type energy-density functionals if the Gogny effective potential is broken down into partial-wave terms. Indeed in such an expansion, the S -wave terms would include the central zero-range t_0 and t_3 terms of the Skyrme effective potential, whereas the P -wave terms would include the central gradient $t_1 + t_2$ SIII term and the zero-range spin-orbit term. It would then be interesting to compare with the corresponding Skyrme terms and to quantify the contribution to ΔE_{GM} of D -wave terms and beyond.

In the framework of mean-field type of approaches, the present study has two main limitations: the nuclear shapes are restricted by intrinsic axial and parity symmetries on the one hand, and particle-number nonconserving treatment of pairing correlations on the other hand. Indeed some nuclei fall in mass regions of observed octupole deformation, essentially the $A \approx 230$ nuclei considered here. The case of ^{154}Eu is unclear as this nucleus does exhibit parity doublet bands but static octupole deformation is not supported according to Ref. [22]. However, octupole vibrations should play a role in the low-energy structure of this odd-odd nucleus [8]. In contrast,

no triaxial static deformation is expected in the considered sample of nuclei. Therefore a natural extension of the present study is to repeat the above analysis with axial and reflection-asymmetric Skyrme-EDF solutions. Regarding the treatment of pairing correlations, it is known that particle-number non-conserving Bogoliubov approach, including its presently used BCS approximation, fail in weak pairing regimes. This happens in particular in BCS calculations with the blocking procedure because the blocked energy levels are excluded from pairing correlations. This calls for a particle-number conserving description of multiquasiparticle states, such as the particle-number projection [55–61], an equation-of-motion method for the pairing-density matrix operators in Heisenberg representation [62], or a multiparticle-multihole configuration mixing [63–65].

More generally the coupling of single-particle and collective motions is not taken into account in our approach and contributes in the structure of low-lying states of odd-odd nuclei. That is especially true for $K = 0$ states. They deserve to be addressed to assess their potential role in the Gallagher-Moszkowski splitting mechanism. This could be done in a fully microscopic way within the generator coordinate method based on symmetry-restored mean-field intrinsic states based on the Gogny EDF [66,67], the Skyrme EDF [68–70], the covariant density functional theory [71–73], or in an *ab initio* framework [74], but this is challenging from the computational point of view. A simpler approach would be a semimicroscopic framework relying on the Bohr-Mottelson unified model in which the intrinsic wave function would be, for example, of the Hartree-Fock-Bogoliubov type (at the price of some redundancy in the collective variables). This framework would allow to incorporate at once the core polarization in the intrinsic wave functions and the particle-rotation, particle-vibration, rotation-vibration couplings, hence restoring intrinsic symmetry breaking in a less demanding way than in the fully microscopic approach.

Finally, despite the above mentioned limitations, the present work, through the evidenced mechanism of Sec. IV, may serve to put constraints on the parameters entering the time-odd terms of the Skyrme energy-density functional. Moreover the study of excitation energies of nuclear states of multiquasiparticle nature, as done in this paper, may provide information on the ordering of the single-particle levels which is important to identify the location of deformed magic numbers. This is especially relevant in the rare-earth region to locate waiting points in the nucleosynthesis r process.

ACKNOWLEDGMENTS

We thank Prof. Philippe Quentin for his reading of the manuscript. This work is partly supported by CNRS and the Bulgarian National Science Fund (BNSF) under Contract No. KP-06-N48/1. M.H.K. would like to acknowledge the French Embassy in Malaysia for financial assistance under the Mobility Programme to Support French-Malaysian Cooperation in Research and Higher Education 2023 to facilitate a research visit at both LP2iB and IHPC.

APPENDIX: DERIVATION OF THE GALLAGHER-MOSZKOWSKI ENERGY SPLITTING IN SKYRME EDF

Let us denote by $\{|\psi_k^{(q)}\rangle, |\psi_{\bar{k}}^{(q)}\rangle, k = 1, 2, \dots\}$ the single-particle (canonical) basis for the charge state $q = n$ (neutrons) or p (protons) in the Skyrme-Hartree-Fock-BCS ground state solution of the underlying even-even $(N - 1, Z - 1)$ nucleus. The state $|\psi_{\bar{k}}^{(q)}\rangle$ is the time-reversed partner of $|\psi_k^{(q)}\rangle$. By convention, the quantum number Ω_k is the positive eigenvalue in \hbar unit of \widehat{J}_z (projection on the z axis of the total angular momentum) for the eigenstate $|\psi_k^{(q)}\rangle$, hence

$$\widehat{J}_z |\psi_k^{(q)}\rangle = \Omega_k |\psi_k^{(q)}\rangle \quad \text{and} \quad \widehat{J}_z |\psi_{\bar{k}}^{(q)}\rangle = -\Omega_k |\psi_{\bar{k}}^{(q)}\rangle. \quad (\text{A1})$$

Owing to time-reversal symmetry, the local spin density $\mathbf{s}_q^{(e-e)}(\mathbf{r})$ in the ground state of this even-even nucleus vanishes:

$$\begin{aligned} \mathbf{s}_q^{(e-e)}(\mathbf{r}) &= \sum_{k>0} v_k^2 (|\psi_k^{(q)}\rangle^\dagger(\mathbf{r}) \boldsymbol{\sigma} |\psi_k^{(q)}\rangle(\mathbf{r})) \\ &+ |\psi_{\bar{k}}^{(q)}\rangle^\dagger(\mathbf{r}) \boldsymbol{\sigma} |\psi_{\bar{k}}^{(q)}\rangle(\mathbf{r})) = 0, \end{aligned} \quad (\text{A2})$$

where $|\psi_k\rangle(\mathbf{r})$ is the spinor at the space point of coordinate vector \mathbf{r} associated with the state $|\psi_k\rangle$, v_k^2 are the BCS occupation probabilities such that $\sum_{k>0} v_k^2 = N - 1$ or $Z - 1$ according to the charge index q , and $\boldsymbol{\sigma} = (\sigma_x, \sigma_y, \sigma_z)$ is the triplet of Pauli matrices.

In the odd-odd nucleus (N, Z) described by perturbative blocking, the local spin density $\mathbf{s}_q^{(o-o)}(\mathbf{r})$ takes the simple form

$$\mathbf{s}_q^{(o-o)}(\mathbf{r}) = \mathbf{s}_q^{(e-e)}(\mathbf{r}) + \mathbf{s}_q^{(i_q)}(\mathbf{r}) = \mathbf{s}_q^{(i_q)}(\mathbf{r}), \quad (\text{A3})$$

where the index i_q of the blocked state denotes either an index k_q , hence $\Omega_{i_q} > 0$, or the time-reversed partner \bar{k}_q so that $\Omega_{i_q} < 0$. The individual local spin density $\mathbf{s}_q^{(i_q)}(\mathbf{r})$ is the contribution from the unpaired, blocked state $|\psi_{i_q}^{(q)}\rangle$

$$\mathbf{s}_q^{(i_q)}(\mathbf{r}) = |\psi_{i_q}^{(q)}\rangle^\dagger(\mathbf{r}) \boldsymbol{\sigma} |\psi_{i_q}^{(q)}\rangle(\mathbf{r}). \quad (\text{A4})$$

Because of the time-odd character of the spin density, we have

$$\mathbf{s}_q^{(\bar{k}_q)}(\mathbf{r}) = -\mathbf{s}_q^{(k_q)}(\mathbf{r}). \quad (\text{A5})$$

It is worth recalling that, by definition of the local spin density, the integral over space of its component along the z axis (nucleus's symmetry axis) is twice the expectation value of the projection \widehat{S}_z of the spin angular momentum (in \hbar unit)

$$\int d^3\mathbf{r} s_{z,q}^{(i_q)}(\mathbf{r}) = 2 \langle \psi_{i_q}^{(q)} | \widehat{S}_z | \psi_{i_q}^{(q)} \rangle. \quad (\text{A6})$$

Let us call $|q\rangle$ the state among the Kramers degenerate pair of states $|\psi_{k_q}^{(q)}\rangle$ and $|\psi_{\bar{k}_q}^{(q)}\rangle$ such that $\langle q | \widehat{S}_z | q \rangle > 0$. The actual blocked state of charge q is thus either $|q\rangle$ or its time-reversed partner $|\bar{q}\rangle$. Then we call \mathbf{s}_q the local spin density of the state $|q\rangle$. Regardless of the Ω_n and Ω_p quantum numbers, we thus have by construction $\langle n | \widehat{S}_z | n \rangle \times \langle p | \widehat{S}_z | p \rangle > 0$. According to Ref. [17], this leads to $\int d^3\mathbf{r} \mathbf{s}_n \cdot \mathbf{s}_p > 0$. In the Gallagher-Moszkowski doublet built from the neutron $|\psi_{i_n}^{(n)}\rangle$ and proton $|\psi_{i_p}^{(p)}\rangle$ blocked states, the spin-aligned configuration has a

total local spin density $\mathbf{s}_{\uparrow\uparrow} = \mathbf{s}_n + \mathbf{s}_p$ or $\mathbf{s}_{\downarrow\downarrow} = -\mathbf{s}_{\uparrow\uparrow}$, while the spin-antialigned configuration has a total local spin density $\mathbf{s}_{\uparrow\downarrow} = \mathbf{s}_n - \mathbf{s}_p$ or $\mathbf{s}_{\downarrow\uparrow} = -\mathbf{s}_{\uparrow\downarrow}$. As will be clear below, both cases of spin alignment and spin antialignment lead to the same expression of ΔE_{GM} because of its bilinear character. We thus choose the combinations $\mathbf{s}_{\uparrow\uparrow}$ and $\mathbf{s}_{\uparrow\downarrow}$. Similar expressions can be derived for the current density, defined for a single-particle state $|\psi_{i_q}^{(q)}\rangle$ by

$$\mathbf{j}_q^{(i_q)}(\mathbf{r}) = \text{Im}([\psi_{i_q}^{(q)}]^\dagger(\mathbf{r})\nabla[\psi_{i_q}^{(q)}](\mathbf{r})). \quad (\text{A7})$$

We have $\mathbf{j}_{\uparrow\uparrow} = \mathbf{j}_n + \mathbf{j}_p$ in the spin-aligned configuration, and $\mathbf{j}_{\uparrow\downarrow} = \mathbf{j}_n - \mathbf{j}_p$. For the Skyrme EDF in the minimal scheme (see Sec. II) we thus obtain the following expression of ΔE_{GM} in such a perturbative-blocking approach:

$$\Delta E_{\text{GM}} = \int d^3\mathbf{r} [(B_{10} + B_{12}\rho^\alpha)(\mathbf{s}_{\uparrow\downarrow}^2 - \mathbf{s}_{\uparrow\uparrow}^2) - B_3(\mathbf{j}_{\uparrow\downarrow}^2 - \mathbf{j}_{\uparrow\uparrow}^2)] + B_9(\mathbf{s}_{\uparrow\downarrow} \cdot \nabla \times \mathbf{j}_{\uparrow\downarrow} - \mathbf{s}_{\uparrow\uparrow} \cdot \nabla \times \mathbf{j}_{\uparrow\uparrow}). \quad (\text{A8})$$

After substitution of the spin-aligned and spin-antialigned local spin and current densities the energy splitting ΔE_{GM} becomes

$$\Delta E_{\text{GM}} = -4 \int d^3\mathbf{r} [(B_{10} + B_{12}\rho^\alpha)\mathbf{s}_n \cdot \mathbf{s}_p - B_3\mathbf{j}_n \cdot \mathbf{j}_p] - 2B_9 \int d^3\mathbf{r} (\mathbf{s}_n \cdot \nabla \times \mathbf{j}_p + \mathbf{s}_p \cdot \nabla \times \mathbf{j}_n). \quad (\text{A9})$$

The energy-density functional coupling constants B_3 , B_9 , B_{10} , and B_{12} are related to the Skyrme SIII parameters by (see Table IX of Ref. [19] or Ref. [54], with $x_1 = x_2 = 0$, $x_3 = 1$)

$$B_3 = \frac{1}{4}(t_1 + t_2), \quad B_9 = -\frac{W}{2}, \\ B_{10} = \frac{1}{4}t_0x_0, \quad B_{12} = \frac{1}{24}t_3. \quad (\text{A10})$$

This leads to

$$\Delta E_{\text{GM}} = \Delta E_{\text{GM}}^{(t_0)} + \Delta E_{\text{GM}}^{(t_3)} + \Delta E_{\text{GM}}^{(t_1+t_2)} + \Delta E_{\text{GM}}^{(W)} \quad (\text{A11})$$

where

$$\Delta E_{\text{GM}}^{(t_0)} = -t_0x_0 \int d^3\mathbf{r} \mathbf{s}_n \cdot \mathbf{s}_p, \quad (\text{A12a})$$

$$\Delta E_{\text{GM}}^{(t_3)} = -\frac{t_3}{6} \int d^3\mathbf{r} \rho^\alpha \mathbf{s}_n \cdot \mathbf{s}_p, \quad (\text{A12b})$$

$$\Delta E_{\text{GM}}^{(t_1+t_2)} = (t_1 + t_2) \int d^3\mathbf{r} \mathbf{j}_n \cdot \mathbf{j}_p, \quad (\text{A12c})$$

$$\Delta E_W = W \int d^3\mathbf{r} (\mathbf{s}_n \cdot \nabla \times \mathbf{j}_p + \mathbf{s}_p \cdot \nabla \times \mathbf{j}_n). \quad (\text{A12d})$$

It is possible to go further in the analysis of the contributions to ΔE_{GM} of each term of the Skyrme effective potential if we approximate the neutron spin-up state $|n\rangle$ and proton spin-up state $|p\rangle$ of the corresponding blocked levels (see their definition above) by the dominant axially deformed harmonic-oscillator basis state:

$$|q\rangle = |\psi_{i_q}^{(q)}\rangle \approx C_{i_q}^{(q)} |N_q n_{z,q} \Lambda_q \Sigma_q\rangle \quad (q = n \text{ or } p), \quad (\text{A13})$$

where $C_{i_q}^{(q)}$ is the expansion coefficient and by definition $\Sigma_q = 1/2$. It is worth recalling that either $i_q = k_q$, in which case $\Omega_{i_q} = \Lambda_q + \Sigma_q > 0$, or $i_q = \bar{k}_q$, in which case $\Omega_{i_q} = \Lambda_q + \Sigma_q < 0$. The Nilsson quantum numbers N_q , $n_{z,q}$, Λ_q , and Σ_q of the dominant harmonic-oscillator basis state in the actual neutron and proton blocked states, together with the weights $|C_{i_q}^{(q)}|^2$, are given in Table I. The wave function of the spatial part $|N n_z \Lambda\rangle$ of the harmonic-oscillator basis state in cylindrical coordinates (ρ, φ, z) is given by

$$\Psi_{N n_z \Lambda}(\rho, \varphi, z) = \mathcal{N} \tilde{H}_{n_z}(\xi) \tilde{L}_{n_r}^{(|\Lambda|)}(\eta) e^{i\Lambda\varphi}, \quad (\text{A14})$$

where $\xi = \beta_z z$, $\eta = (\beta_\perp \rho)^2$, $2n_r + |\Lambda| = N - n_z$, $\tilde{H}_n(\xi) = e^{-\xi^2 \beta_z^2/2} H_n(\xi)$, $\tilde{L}_{n_r}^{(|\Lambda|)}(\eta) = e^{-\eta/2} \eta^{|\Lambda|/2} L_{n_r}^{(|\Lambda|)}(\eta)$, and \mathcal{N} is a real normalization coefficient. Because $\langle \Sigma | \sigma_x | \Sigma \rangle = \Sigma$ and $\langle \Sigma | \sigma_y | \Sigma \rangle = 0$, we can thus deduce the following approximate expression for the local spin density associated with the single-particle state $|q\rangle$ of Eq. (A13):

$$\mathbf{s}_q^{(i_q)}(\mathbf{r}) = |C_{i_q}^{(q)}|^2 (\mathcal{N}_q \tilde{H}_{n_{z,q}}(\xi) \tilde{L}_{n_{r,q}}^{(|\Lambda|)}(\eta))^2 \Sigma_q \mathbf{e}_z, \quad (\text{A15})$$

where \mathbf{e}_z is the unit vector of the symmetry axis. The gradient of the harmonic-oscillator wave function $\Psi_{N n_z \Lambda}(\mathbf{r})$, expressed in the orthonormal cylindrical basis $\{\mathbf{e}_\rho, \mathbf{e}_\varphi, \mathbf{e}_z\}$, is given by

$$\nabla \Psi_{N n_z \Lambda}(\mathbf{r}) = \mathcal{N} e^{i\Lambda\varphi} \left[\tilde{H}_{n_z}(\xi) \frac{\partial \tilde{L}_{n_r}^{(|\Lambda|)}}{\partial \rho} \mathbf{e}_\rho + \frac{i\Lambda}{\rho} \tilde{H}_{n_z}(\xi) \tilde{L}_{n_r}^{(|\Lambda|)}(\eta) \mathbf{e}_\varphi + \frac{\partial \tilde{H}_{n_z}}{\partial z} \tilde{L}_{n_r}^{(|\Lambda|)}(\eta) \mathbf{e}_z \right], \quad (\text{A16})$$

therefore the local current density associated with the single-particle state $|q\rangle$ is orthoradial and reads

$$\mathbf{j}_q^{(i_q)}(\mathbf{r}) = |C_{i_q}^{(q)}|^2 \mathcal{N}_q \Lambda_q F_q(\rho, z) \mathbf{e}_\varphi, \quad (\text{A17})$$

where

$$F_q(\rho, z) = \frac{1}{\rho} [\tilde{H}_{n_{z,q}}(\xi) \tilde{L}_{n_{r,q}}^{(|\Lambda_q|)}(\eta)]^2. \quad (\text{A18})$$

As mentioned, above the single-particle $|q\rangle$ is the one among the Kramers degenerate pair of states $|\psi_{k_q}^{(q)}\rangle$ and $|\psi_{\bar{k}_q}^{(q)}\rangle$ such that $\langle q | \hat{S}_z | q \rangle > 0$, therefore we expect that $\Sigma_q > 0$. We can deduce that, in the approximation of Eq. (A13), $\Delta E_{\text{GM}}^{(t_0)}$ and $\Delta E_{\text{GM}}^{(t_3)}$ are proportional to $\Sigma_n \Sigma_p$ (expected to be positive):

$$\Delta E_{\text{GM}}^{(t_0)} \approx -t_0x_0 |C_{i_n}^{(n)}|^2 |C_{i_p}^{(p)}|^2 \Sigma_n \Sigma_p \frac{\pi (\mathcal{N}_n \mathcal{N}_p)^2}{\beta_z \beta_\perp^2} \\ \times \int_{-\infty}^{+\infty} d\xi [\tilde{H}_{n_{z,n}}(\xi) \tilde{H}_{n_{z,p}}(\xi)]^2 \\ \times \int_0^{+\infty} d\eta [\tilde{L}_{n_{r,n}}^{(|\Lambda_n|)}(\eta) \tilde{L}_{n_{r,p}}^{(|\Lambda_p|)}(\eta)]^2 \quad (\text{A19})$$

and

$$\begin{aligned} \Delta E_{\text{GM}}^{(t_3)} &\approx -\frac{t_3}{6} |C_{i_n}^{(n)}|^2 |C_{i_p}^{(p)}|^2 \Sigma_n \Sigma_p \frac{\pi (\mathcal{N}_n \mathcal{N}_p)^2}{\beta_z \beta_\perp^2} \\ &\times \int_{-\infty}^{+\infty} d\xi \int_0^{+\infty} d\eta [\tilde{H}_{n_z, n}(\xi) \tilde{H}_{n_z, p}(\xi)]^2 \\ &\times [\tilde{L}_{n_r, n}^{(\Lambda_n)}(\eta) \tilde{L}_{n_r, p}^{(\Lambda_p)}(\eta)]^2 \rho^\alpha(\mathbf{r}); \end{aligned} \quad (\text{A20})$$

whereas $\Delta E_{\text{GM}}^{(t_1+t_2)}$ is proportional to $\Lambda_n \Lambda_p$:

$$\begin{aligned} \Delta E_{\text{GM}}^{(t_1+t_2)} &\approx (t_1 + t_2) |C_{i_n}^{(n)}|^2 |C_{i_p}^{(p)}|^2 \Lambda_n \Lambda_p \frac{(\mathcal{N}_n \mathcal{N}_p)^2}{2\beta_z \beta_\perp^2} \\ &\times \int_{-\infty}^{+\infty} d\xi [\tilde{H}_{n_z, n}(\xi) \tilde{H}_{n_z, p}(\xi)]^2 \\ &\times \int_0^{+\infty} \frac{d\eta}{\eta} [\tilde{L}_{n_r, n}^{(\Lambda_n)}(\eta) \tilde{L}_{n_r, p}^{(\Lambda_p)}(\eta)]^2. \end{aligned} \quad (\text{A21})$$

To complete this Appendix we also derive the approximate expression of the spin-orbit contribution $\Delta E_{\text{GM}}^{(W)}$. To do so we need to calculate the curl of the current density (A17) in cylindrical coordinates,

$$\nabla \times \mathbf{j}_q^{(i_q)}(\mathbf{r}) = |C_{i_q}^{(q)}|^2 \mathcal{N}_q^2 \Lambda_q \left[\frac{1}{\rho} \frac{\partial}{\partial \rho} (\rho F_q) \mathbf{e}_z - \frac{\partial F_q}{\partial z} \mathbf{e}_\rho \right], \quad (\text{A22})$$

where F_q was defined by Eq. (A18). The dot product of $\nabla \times \mathbf{j}_q^{(i_q)}$ with the spin density thus involves only the z component, and we obtain

$$\begin{aligned} \Delta E_{\text{GM}}^{(W)} &\approx W |C_{i_n}^{(n)}|^2 |C_{i_p}^{(p)}|^2 \frac{2\pi (\mathcal{N}_n \mathcal{N}_p)^2}{\beta_z} \\ &\times \int_{-\infty}^{+\infty} d\xi [\tilde{H}_{n_z, n}(\xi) \tilde{H}_{n_z, p}(\xi)]^2 \\ &\times (\Sigma_n \Lambda_p I_{np} + \Sigma_p \Lambda_n I_{pn}), \end{aligned} \quad (\text{A23})$$

where

$$I_{np} = \int_0^{+\infty} d\eta [\tilde{L}_{n_r, n}^{(\Lambda_n)}(\eta)]^2 \frac{\partial}{\partial \eta} [\tilde{L}_{n_r, p}^{(\Lambda_p)}(\eta)]^2, \quad (\text{A24a})$$

$$I_{pn} = \int_0^{+\infty} d\eta [\tilde{L}_{n_r, p}^{(\Lambda_p)}(\eta)]^2 \frac{\partial}{\partial \eta} [\tilde{L}_{n_r, n}^{(\Lambda_n)}(\eta)]^2. \quad (\text{A24b})$$

Using integration by parts we can relate I_{pn} and I_{np} as

$$I_{pn} + I_{np} = -[\tilde{L}_{n_r, n}^{(\Lambda_n)}(0) \tilde{L}_{n_r, p}^{(\Lambda_p)}(0)]^2 \quad (\text{A25})$$

and then bring $\Delta E_{\text{GM}}^{(W)}$ to the form

$$\begin{aligned} \Delta E_{\text{GM}}^{(W)} &\approx W |C_{i_n}^{(n)}|^2 |C_{i_p}^{(p)}|^2 \frac{2\pi (\mathcal{N}_n \mathcal{N}_p)^2}{\beta_z} \\ &\times \int_{-\infty}^{+\infty} d\xi [H_{n_z, n}(\xi) H_{n_z, p}(\xi)]^2 \\ &\times \{ (\Sigma_p \Lambda_n - \Sigma_n \Lambda_p) I_{pn} \\ &- \Sigma_n \Lambda_p [\tilde{L}_{n_r, n}^{(\Lambda_n)}(0) \tilde{L}_{n_r, p}^{(\Lambda_p)}(0)]^2 \}, \end{aligned} \quad (\text{A26})$$

with $\tilde{L}_{n_r}^{(\Lambda)}(0) = \delta_{\Lambda 0}$ hence $\Lambda \tilde{L}_{n_r}^{(\Lambda)}(0) = 0$. Finally, because Σ_q is expected to be positive, we have $\Sigma_n = \Sigma_p = 12$ and we can simplify $\Delta E_{\text{GM}}^{(W)}$ as

$$\begin{aligned} \Delta E_{\text{GM}}^{(W)} &\approx W |C_{i_n}^{(n)}|^2 |C_{i_p}^{(p)}|^2 \frac{\pi (\mathcal{N}_n \mathcal{N}_p)^2}{\beta_z} \\ &\times (\Lambda_n - \Lambda_p) I_{pn} \int_{-\infty}^{+\infty} d\xi [H_{n_z, n}(\xi) H_{n_z, p}(\xi)]^2. \end{aligned} \quad (\text{A27})$$

Given that $W > 0$, the sign of $\Delta E_{\text{GM}}^{(W)}$ is the sign of $(\Lambda_n - \Lambda_p) I_{pn}$ and depends on the quantum numbers Λ_n , Λ_p as well as $n_{r, n}$ and $n_{r, p}$ through I_{pn} . The integral I_{pn} can be analytically calculated but gives a very complicated function of Λ_n , Λ_p , $n_{r, n}$, and $n_{r, p}$. Therefore the sign of $\Delta E_{\text{GM}}^{(W)}$ is strongly dependent on the nodal and azimuthal structure of the proton and neutron wave functions.

-
- [1] Å. Bohr and B. R. Mottelson, Collective and individual-particle aspects of nuclear structure, *Dan. Mat. Fys. Medd.* **27**, 16 (1953).
- [2] L. K. Peker, *Izv. Akad. Nauk SSSR, Ser. Fiz.* **31**, 1029 (1957).
- [3] C. J. Gallagher and S. A. Moszkowski, Coupling of angular momenta in odd-odd nuclei, *Phys. Rev.* **111**, 1282 (1958).
- [4] J. P. Boisson, R. Piepenbring, and W. Ogle, The effective neutron-proton interaction in rare-earth nuclei, *Phys. Rep.* **26**, 99 (1976).
- [5] N. I. Pyatov, Level splitting in deformed even- A nuclei, *Bull. Acad. Sci. USSR, Phys. Ser.* **27**, 1409 (1964).
- [6] A. G. D. Pinho and J. Picard, Pourquoi la règle de Gallagher–Moszkowski est-elle si bien vérifiée? *Phys. Lett.* **15**, 250 (1965).
- [7] P. Nunberg and D. Prosperi, Neutron-proton residual interaction in odd-odd deformed nuclei, *Nuovo Cimento B* **40**, 318 (1965).
- [8] A. K. Jain, R. K. Sheline, D. M. Headly, P. C. Sood, D. G. Burke, I. Hrivnacova, J. Kvasil, D. Nosek, and R. W. Hoff, Nuclear structure in odd-odd nuclei, $144 \leq A \leq 194$, *Rev. Mod. Phys.* **70**, 843 (1998).
- [9] A. Covello, A. Gargano, and N. Itaco, Tensor force in doubly odd deformed nuclei, *Phys. Rev. C* **56**, 3092 (1997).
- [10] L. M. Robledo, R. N. Bernard, and G. F. Bertsch, Spin constraints on nuclear energy density functionals, *Phys. Rev. C* **89**, 021303(R) (2014).
- [11] D. E. Ward, B. G. Carlsson, P. Möller, and S. Åberg, Global microscopic calculations of odd-odd nuclei, *Phys. Rev. C* **100**, 034301 (2019).
- [12] L. Bennour, J. Libert, M. Meyer, and P. Quentin, A self-consistent description of the spectroscopic properties of odd-odd nuclei, *Nucl. Phys. A* **465**, 35 (1987).

- [13] N. Minkov, L. Bonneau, P. Quentin, J. Bartel, H. Molique, and D. Ivanova, *K*-isomeric states in well-deformed heavy even-even nuclei, *Phys. Rev. C* **105**, 044329 (2022).
- [14] J. A. Maruhn, P.-G. Reinhard, P. D. Stevenson, and A. S. Umar, The TDHF code Sky3D, *Comput. Phys. Commun.* **185**, 2195 (2014).
- [15] N. Schunck, J. Dobaczewski, P. B. W. Satuła, J. Dudek, Y. Gao, M. Konieczka, K. Sato, Y. Shi, X. B. Wang, and T. R. Werner, Solution of the Skyrme-Hartree-Fock-Bogolyubov equations in the Cartesian deformed harmonic-oscillator basis. (VIII) HFODD (v2.73y): A new version of the program, *Comput. Phys. Commun.* **216**, 145 (2017).
- [16] W. Ryssens and M. Bender, Skyrme pseudopotentials at next-to-next-to-leading order: Construction of local densities and first symmetry-breaking calculations, *Phys. Rev. C* **104**, 044308 (2021).
- [17] L. Bonneau, N. Minkov, D. D. Duc, P. Quentin, and J. Bartel, Effect of core polarization on magnetic dipole moments in deformed odd-mass nuclei, *Phys. Rev. C* **91**, 054307 (2015).
- [18] M. Beiner, H. Flocard, N. V. Giai, and P. Quentin, Nuclear ground-state calculations properties and self-consistent with the Skyrme interaction, *Nucl. Phys. A* **238**, 29 (1975).
- [19] M.-H. Koh, L. Bonneau, P. Quentin, T. V. Nhan Hao, and H. Wagiran, Fission barriers of two odd-neutron actinide nuclei taking into account the time-reversal symmetry breaking at the mean-field level, *Phys. Rev. C* **95**, 014315 (2017).
- [20] N. M. Nor, N.-A. Rezle, K.-W. Kelvin-Lee, M.-H. Koh, L. Bonneau, and P. Quentin, Consistency of two different approaches to determine the strength of a pairing residual interaction in the rare-earth region, *Phys. Rev. C* **99**, 064306 (2019).
- [21] H. Flocard, P. Quentin, A. K. Kerman, and D. Vautherin, Nuclear deformation energy curves with the constrained Hartree-Fock method, *Nucl. Phys. A* **203**, 433 (1973).
- [22] A. V. Afanasjev and I. Ragnarsson, Existence of intrinsic reflection-asymmetry at low spin in odd and odd-odd mass nuclei in the Pm/Eu region, *Phys. Rev. C* **51**, 1259 (1995).
- [23] S. E. Agbemava, A. V. Afanasjev, and P. Ring, Octupole deformation in the ground state of even-even nuclei: A global analysis within the covariant density functional theory, *Phys. Rev. C* **93**, 044304 (2016).
- [24] Y. Cao, S. E. Agbemava, A. V. Afanasjev, W. Nazarewicz, and E. Olsen, Landscape of pear-shaped even-even nuclei, *Phys. Rev. C* **102**, 024311 (2020).
- [25] N. Nica, Nuclear data sheets for $A = 158$, *Nucl. Data Sheets* **141**, 1 (2017).
- [26] M. K. Balodis, J. J. Tambergs, K. J. Alksnis, P. T. Prokofjev, W. G. Vonach, H. K. Vonach, H. R. Koch, U. Gruber, B. P. K. Maier, and O. W. B. Schult, The level scheme of ^{176}Lu investigated by (n, γ) and (n, e) reactions, *Nucl. Phys. A* **194**, 305 (1972).
- [27] N. Klay, F. Käppeler, H. Beer, G. Schatz, H. Borner, F. Hoyler, S. J. Robinson, K. Schreckenbach, B. Krusche, U. Mayerhofer, G. Hlawatsch, H. Lindner, T. von Egidy, W. Andrejtscheff, and P. Petkov, Nuclear structure of ^{176}Lu and its astrophysical consequences. I. Level scheme of ^{176}Lu , *Phys. Rev. C* **44**, 2801 (1991).
- [28] E. Achterberg, O. A. Capurro, and G. V. Marti, Nuclear data sheets for $A = 178$, *Nucl. Data Sheets* **110**, 1473 (2009).
- [29] F. G. Kondev, M. Wang, W. J. Huang, S. Naimi, and G. Audi, The NUBASE2020 evaluation of nuclear physics properties, *Chin. Phys. C* **45**, 030001 (2021).
- [30] J. F. C. Cocks, D. Hawcroft, N. Amzal, P. A. Butler, K. J. Cann, P. T. Greenlees, G. D. Jones, S. Asztalos, R. M. Clark, M. A. Deleplanque, R. M. Diamond, P. Fallon, I. Y. Lee, A. O. Macchiavelli, R. W. MacLeod, P. S. Stephens, P. Jones, R. Julin, R. Broda, B. Fornal *et al.*, Spectroscopy of Rn, Ra and Th isotopes using multi-nucleon transfer reactions, *Nucl. Phys. A* **645**, 61 (1999).
- [31] T. Kotthaus, P. Reiter, H. Hess, M. Kalkühler, A. Wendt, A. Wiens, R. Hertenberg, T. Morgan, P. G. Thirolf, H.-F. Wirth, and T. Faestermann, Excited states of the odd-odd nucleus ^{230}Pa , *Phys. Rev. C* **87**, 044322 (2013).
- [32] C. W. Reich, Nuclear data sheets for $A = 154$, *Nucl. Data Sheets* **110**, 2257 (2009).
- [33] H. Rotter, C. Heiser, K. D. Schilling, L. K. K. W. Andrejtscheff, and M. K. Balodis, Electromagnetic transition probabilities in the doubly odd $N = 91$ nucleus ^{154}Eu , *Nucl. Phys. A* **417**, 1 (1984).
- [34] M. K. Balodis, P. T. Prokofjev, N. D. Kramer, L. I. Simonova, K. Schreckenbach, W. F. Davidson, J. A. Pinston, P. Hungerford, H. H. Schmidt, H. J. Scheerer, T. von Egidy, P. H. M. van Assche, A. M. J. Spits, R. F. Casten, W. R. Kane, D. D. Warner, and J. Kern, Levels in ^{154}Eu populated by (n, γ) and (d, p) reactions, *Nucl. Phys. A* **472**, 445 (1987).
- [35] C. W. Reich, Nuclear data sheets for $A = 156$, *Nucl. Data Sheets* **113**, 2537 (2012).
- [36] N. Nica, Nuclear data sheets for $A = 160$, *Nucl. Data Sheets* **176**, 1 (2021).
- [37] B. Singh, Nuclear data sheets for $A = 172$, *Nucl. Data Sheets* **75**, 199 (1995).
- [38] R. O. Hughes, G. J. Lane, G. D. Dracoulis, T. Kibédi, P. Nieminen, and H. Watanabe, Two-quasiparticle isomer, $E1$ hindrances and residual interactions in ^{172}Tm , *Phys. Rev. C* **77**, 044309 (2008).
- [39] E. Browne and H. Junde, Nuclear data sheets for $A = 174$, *Nucl. Data Sheets* **87**, 15 (1999).
- [40] M. S. Basunia, Nuclear data sheets for $A = 176$, *Nucl. Data Sheets* **107**, 791 (2006).
- [41] D. G. Burke, P. C. Sood, P. E. Garrett, T. Qu, R. K. Sheline, and R. W. Hoff, Nuclear structure of ^{178}Lu , *Phys. Rev. C* **47**, 131 (1993).
- [42] F. Kondev, G. D. Dracoulis, A. P. Byrne, and T. Kibédi, Intrinsic states and rotational bands in ^{176}Ta and ^{178}Ta , *Nucl. Phys. A* **632**, 473 (1998).
- [43] E. A. McCutchan, Nuclear data sheets for $A = 180$, *Nucl. Data Sheets* **126**, 151 (2015).
- [44] E. Browne and J. K. Tuli, Nuclear data sheets for $A = 230$, *Nucl. Data Sheets* **113**, 2113 (2012).
- [45] E. Browne and J. K. Tuli, Nuclear data sheets for $A = 234$, *Nucl. Data Sheets* **108**, 681 (2007).
- [46] J. Godart and A. Gizon, Niveaux de ^{234}Pa atteints par la désintégration de ^{234}Th , *Nucl. Phys. A* **217**, 159 (1973).
- [47] A. G. D. Pinho and J. Picard, Les bandes de rotation $K = 0^-$ et $K = 1^-$ dans le ^{234}Pa , *Nucl. Phys.* **65**, 426 (1965).
- [48] E. Browne and J. K. Tuli, Nuclear data sheets for $A = 238$, *Nucl. Data Sheets* **127**, 191 (2015).
- [49] E. Browne and J. K. Tuli, Nuclear data sheets for $A = 240$, *Nucl. Data Sheets* **109**, 2657 (2008).
- [50] M. J. Martin and C. D. Nesaraja, Nuclear Data Sheets for $A = 242$, *Nucl. Data Sheets* **186**, 263 (2022).

- [51] C. D. Nesaraja, Nuclear data sheets for $A = 244$, *Nucl. Data Sheets* **146**, 387 (2017).
- [52] T. von Egidy, R. W. Hoff, R. W. Logheed, D. H. White, H. G. Börner, K. Schreckenbach, D. D. Warner, G. Barreau, and P. Hungerford, Nuclear structure of ^{244}Am investigated with the (n, γ) reaction, *Phys. Rev. C* **29**, 1243 (1984).
- [53] Y. A. Akovali, Nuclear data sheets for $A = 250$, *Nucl. Data Sheets* **94**, 131 (2001).
- [54] V. Hellema, P.-H. Heenen, and M. Bender, Tensor part of the Skyrme energy density functional. III. Time-odd terms at high spin, *Phys. Rev. C* **85**, 014326 (2012).
- [55] K. Dietrich, H. J. Mang, and J. H. Pradal, Conservation of particle number in the nuclear pairing model, *Phys. Rev.* **135**, B22 (1964).
- [56] J. L. Egidio and P. Ring, Symmetry conserving Hartree-Fock-Bogoliubov theory (I). On the solution of variational equations, *Nucl. Phys. A* **383**, 189 (1982).
- [57] P.-H. Heenen, P. Bonche, J. Dobaczewski, and H. Flocard, Generator-coordinate method for triaxial quadrupole dynamics in Sr isotopes (II). Results for particle-number projected states, *Nucl. Phys. A* **561**, 367 (1993).
- [58] M. Bender and P.-H. Heenen, Configuration mixing of angular-momentum and particle-number projected triaxial Hartree-Fock-Bogoliubov states using the Skyrme energy-density functional, *Phys. Rev. C* **78**, 024309 (2008).
- [59] M. Bender, T. Duguet, and D. Lacroix, Particle-number restoration within the energy density functional formalism, *Phys. Rev. C* **79**, 044319 (2009).
- [60] C. Simenel, Particle transfer reactions with the time-dependent Hartree-Fock theory using a particle-number projection technique, *Phys. Rev. Lett.* **105**, 192701 (2010).
- [61] T. R. Rodriguez and J. L. Egidio, Configuration mixing description of the nucleus ^{44}S , *Phys. Rev. C* **84**, 051307(R) (2011).
- [62] L. Y. Jia, Particle-number-conserving theory for nuclear pairing, *Phys. Rev. C* **88**, 044303 (2013).
- [63] J. Y. Zeng and T. S. Cheng, Particle-number-conserving method for treating the nuclear pairing correlation, *Nucl. Phys. A* **405**, 1 (1983).
- [64] N. Pillet, P. Quentin, and J. Libert, Pairing correlations in an explicitly particle-number conserving approach, *Nucl. Phys. A* **697**, 141 (2002).
- [65] N. Pillet, J.-F. Berger, and E. Caurier, Variational multiparticle-multihole configuration mixing method applied to pairing correlations in nuclei, *Phys. Rev. C* **78**, 024305 (2008).
- [66] L. M. Robledo, T. R. Rodríguez, and R. R. Rodríguez-Guzmán, Mean field and beyond description with the Gogny force: A review, *J. Phys. G: Nucl. Part. Phys.* **46**, 013001 (2019).
- [67] R. R. Rodríguez-Guzmán and L. M. Robledo, Beyond-mean-field description of octupolarity in dysprosium isotopes with the Gogny-DIM energy density functional, *Phys. Rev. C* **108**, 024301 (2023).
- [68] B. Bally, B. Avez, M. Bender, and P. H. Heenen, Beyond mean-field calculations for odd-mass nuclei, *Phys. Rev. Lett.* **113**, 162501 (2014).
- [69] B. Bally and M. Bender, Projection on particle number and angular momentum: Example of triaxial Bogoliubov quasiparticle states, *Phys. Rev. C* **103**, 024315 (2021).
- [70] B. Bally, G. Giacalone, and M. Bender, The shape of gold, *Eur. Phys. J. A* **59**, 58 (2023).
- [71] P. W. Zhao, P. Ring, and J. Meng, Configuration interaction in symmetry-conserving covariant density functional theory, *Phys. Rev. C* **94**, 041301(R) (2016).
- [72] K. Wang and B.-N. Lu, Angular momentum and parity projected multidimensionally constrained relativistic Hartree-Bogoliubov model, *Commun. Theor. Phys.* **74**, 015303 (2022).
- [73] E. F. Zhou and J. M. Yao, Generator coordinate method for nuclear octupole excitations: Status and perspectives, *Int. J. Mod. Phys. E* **32**, 2340011 (2023).
- [74] M. Frosini, T. Duguet, J. P. Ebran, and V. Somà, Multi-reference many-body perturbation theory for nuclei, *Eur. Phys. J. A* **58**, 62 (2022).